ACS OMEGA

Open Access

http://pubs.acs.org/journal/acsodf

Article

Actinobacterium-Mediated Green Synthesis of CuO/Zn−Al LDH Nanocomposite Using *Micromonospora* sp. ISP-2 27: A Synergistic Study that Enhances Antimicrobial Activity

Abdullah A. Eweis, Maged S. Ahmad, Ehab B. El Domany, Mohammed Al-Zharani, Mohammed Mubarak, Zienab E Eldin, Yasser GadelHak, Rehab Mahmoud,* and Wael N. Hozzein

Cite This: *ACS Omega* 2024, 9, 34507−34529

Read Online

ACCESS | Metrics & More | Article Recommendations

ABSTRACT: Bacterial resistance to conventional antibiotics has created an urgent need to develop enhanced alternatives. Nanocomposites combined with promising antibacterial nanomaterials can show improved antimicrobial activity compared to that of their components. In this work, green synthesized CuO nanoparticles (NPs) supported on an anionic clay with a hydrotalcite-like structure such as Zn−Al layered double hydroxide (LDH) nanocomposite were investigated as antimicrobial agents. This nanocomposite was synthesized using *Micromonospora* sp. ISP-2 27 cell-free supernatant to form CuO NPs on the surface of previously synthesized LDH. The prepared samples were characterized using UV−Vis spectrophotometry, XRD, FTIR, Field emission scanning electron microscopy with EDX, zeta potential, and hydrodynamic particle size. UV−vis spectral analysis of the biosynthesized CuO NPs revealed a maximum peak at 300 nm, indicating their successful synthesis. The synthesized CuO NPs had a flower-like morphology with a size range of 43−78 nm, while the LDH support had a typical hexagonal layered structure. The zeta potentials of the CuO NPs, Zn−Al LDH, and CuO NPs/LDH nanocomposite were −21.4, 22.3, and 30.8 mV, respectively, while the average hydrodynamic sizes were 687, 735, and 528 nm, respectively. The antimicrobial activity of the produced samples was tested against several microbes. The results demonstrated that the nanocomposite displayed superior antimicrobial properties compared to those of its components. Among the microbes tested, *Listeria monocytogenes* ATCC 7644 was more sensitive (30 ± 0.34) to the biosynthesized nanocomposite than to CuO NPs (25 ± 0.05) and Zn−Al LDH (22 ± 0.011). In summary, the use of nanocomposites with superior antimicrobial properties has the potential to offer innovative solutions to the global challenge of antibiotic resistance by providing alternative treatments, reducing the reliance on traditional antibiotics, and contributing to the development of more effective and targeted therapeutic approaches.

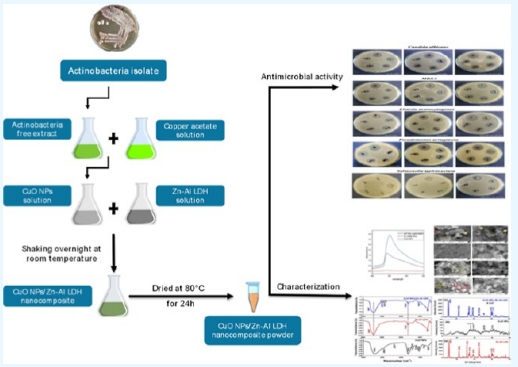

1. INTRODUCTION

The increasing antibiotic resistance of pathogenic organisms can be considered one of the most significant problems facing humanity.[1] This resistance can be attributed to several factors, such as the enzymatic degradation of antibiotics, decreased drug uptake, mutation in the drug target site, drug inactivation, and active efflux through permeability barriers.[2,3] To combat such resistance, numerous pathways are available, such as modifying antibiotic targets, improving drug release, decreasing the consumption of antimicrobial compounds, and developing novel antimicrobial medicines.[4] Recently, nanotechnology has emerged as a useful tool in numerous biomedical applications. Novel nanomaterials and nanocomposites have shown promising antibacterial,[5,6] antifungal,[7,8] and antiviral[9,10] effects against numerous pathogens. Compared with those of their bulk materials, the unique properties of nanomaterials can enhance their antibacterial properties and allow for their application as antibacterial agents.[11] Furthermore, nanomaterials possess unique characteristics that make them effective at combating antibiotic resistance. The high surface area-to-volume ratio, thermal and chemical stability, and optimized physicochemical properties of these materials allow them to overcome the limitations of traditional therapies and provide prolonged protection against harmful microorganisms.[12,13] These nanoparticles have the ability to disrupt the cell walls or membranes of bacteria, effectively eliminating strains that have developed resistance.[14,15] They can also specifically target biofilms and eradicate infections that are difficult to treat.[16] Certain

Received: March 14, 2024
Revised: July 25, 2024
Accepted: July 26, 2024
Published: August 2, 2024

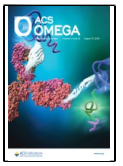

nanoparticles, such as silver, copper, gold, zinc oxide, and iron oxide, have demonstrated remarkable antimicrobial properties and use nonspecific mechanisms to kill bacteria, preventing the development of resistance.[17] Additionally, nanoparticles possess advantageous characteristics, including active targeting, prolonged binding, and protection against enzymes, thereby facilitating elevated antibiotic concentrations within cells and diminishing the necessity for increased dosages, consequently mitigating detrimental consequences.[18] In addition, compared with traditional antibiotics, nanomaterials may be less prone to triggering resistance in bacteria. Therefore, compared with traditional antibiotics,[19] nanomaterials are advantageous for combating microbial resistance because they can bypass antibiotic resistance mechanisms and target biofilms, which are difficult to treat.[17] Additionally, nanomaterials provide advantages over traditional antibiotics by offering sustained release, targeted delivery, and reduced dosing frequency, which can help combat microbial resistance.[20] Additionally, nanoparticles have a high surface area-to-volume ratio, which enhances their antimicrobial activity, providing an effective alternative to traditional antibiotics.[12]

The main families of nanomaterials that have been investigated for their antibacterial properties are metals, metal oxides (MO), and carbonaceous nanomaterials. Silver nanoparticles, one of the most studied metal-based nanomaterials, can be considered highly effective antibacterial agents that can inhibit the growth of numerous pathogenic microorganisms, including highly resistant strains, at very low concentrations, showing no cytotoxicity to mammalian cells.[21] In addition, gold nanoparticles with different particle sizes, dispersibilities, and surface modifications have shown promising antibacterial properties.[22] Other metal nanoparticles, such as zerovalent iron,[23−25] copper,[26,27] zinc,[28,29] bismuth,[30,31] nickel,[32−34] and cobalt,[35,36] have been tested. These metal nanoparticles, in general, have antibacterial effects via different mechanisms, such as cation release based on their oxidation susceptibility, Reactive Oxygen Species (ROS) production, biomolecule damage, membrane interactions, and ATP depletion.[37]

In addition to metals, MO nanomaterials have also attracted wide interest as possible antimicrobial agents. For instance, copper oxide nanoparticles, one of the most widely studied metal oxide nanoparticles, were reported to possess high activity against staphylococcal biofilm formation and to cause bacterial leakage of the cellular content of methicillin-resistant *Staphylococcus aureus*.[21] Generally, CuO is widely studied due to its superior antibacterial properties, which render it the most toxic to Gram-positive bacteria such as *Bacillus subtilis*, among other oxides such as NiO, ZnO, and Sb_2O_3.[38] Magnesium and calcium oxide nanoparticles were also reported to possess strong antibacterial properties due to their high alkalinity and ability to produce ROS.[21] Other MO, such as zinc oxide,[39,40] nickel oxide,[41,42] iron oxide,[43−45] cobalt oxide,[46−48] and aluminum oxide,[49] have been investigated for their antibacterial properties. In addition to metals and MO, carbon-based nanomaterials, such as graphene,[50,51] graphene oxide,[52−54] and carbon nanotubes,[55,56] have also been investigated. However, such nanomaterials are usually more expensive to produce and require complicated synthesis procedures and/or hazardous chemicals.

In addition to the above-mentioned families of nanomaterials, layered double hydroxides (LDHs) have emerged as promising 2D nanomaterials for numerous applications. LDH, popularly called anionic clay, has a hydrotalcite-like structure that can be obtained naturally in the form of minerals and is also easily synthesized in the laboratory.[57] LDHs are 2D structural materials with the general formula $[(M^{II})_{1-x}(M^{III})_x(OH)_2]^{x+}(A^{m-}{}_{x/m})\cdot nH_2O]$, where M^{II} refers to divalent cations such as Ni^{2+}, Zn^{2+}, Mg^{2+}, and Co^{2+}; M^{III} refers to trivalent cations such as Al^{3+}, Fe^{3+}, and Cr^{3+}; and A^{m-} is considered an active anion such as Cl^-, $NO_3{}^-$, and $CO_3{}^-$.[58] The remarkable properties of LDHs, such as their special layered structure, significant anion substitution capacity, high surface area, and high thermal stability, make them promising candidates for a wide range of applications, including as catalysts, photoresponsive materials, and drug carriers.[59] Recent papers published in the open literature have investigated the antibacterial properties of LDH materials such as CuAl,[60,61] MgAl,[61−63] NiAl,[61] ZnFe,[64,65] ZnMgFe,[66] CoNiZnFe,[67] CoAl,[61] CuZnAl,[68] and ZnAl.[61,69]

One of the approaches to enhancing the antibacterial properties of such nanomaterials is to combine two or more members of a nanocomposite, such as metal/MO,[70−72] MO/LDH, or M/LDH,[73−75] which can result in higher activity than the individual constituents of the composite. The combinations of nanomaterials play a crucial role in today's scientific research due to their potential to yield innovative properties and functions that are distinct from those of their constituent elements. By merging different nanoscale materials, these hybrid nanostructures, also known as nanocomposites, effectively integrate the various functionalities and advantages of multiple nanoscale materials into a single nanoobject. This integration of diverse materials at the nanoscale level opens up new avenues for material design and engineering, paving the way for the development of advanced technologies and applications.[76] One of the challenges with metal synthesis is that it can be prone to oxidation after production and during storage, which will alter its chemical structure and hence its properties.[77,78] Therefore, MO/LDH nanocomposites can be regarded as simple, cost-effective, and promising types of nanocomposites for use as antibacterial agents. No previous work has attempted to study the antibacterial properties of such composites. Rasouli et al. prepared such a composite but calcined the product at 500 °C to transform the LDH phase into the corresponding mixed metal oxide.[79] However, the calcination step can be regarded as an expensive step that can increase the overall cost of the product, and in this work, the chemical structure of LDH was preserved with no oxidation. In this work, CuO was chosen to represent the oxide phase, while ZnAl was used as the model LDH support. This work represents the first study to investigate the antibacterial properties of MO/LDH nanocomposites. Future work can be conducted to investigate more combinations of the MO and LDH phases to optimize the antibacterial activity against various pathogens.

The investigation of nanomaterials for antibacterial applications has yielded promising outcomes in current research. However, there is a noticeable gap in the literature in regard to exploring the antibacterial properties of MO/LDH (metal oxide/LDH) nanocomposites. To the best of our knowledge, there has been limited comprehensive exploration into the synergistic effects and unique attributes that MO/LDH nanocomposites may possess in the context of combating bacterial infections. The novelty of our study lies in its specific focus on MO/LDH nanocomposites, which combine the advantageous properties of MO and LDHs (LDH). Although both MO[42,43,48] and LDHs[60,62,64] have individually exhibited antibacterial potential, the synergistic interactions and enhanced efficacy resulting from their combination remain largely

https://doi.org/10.1021/acsomega.4c02133
ACS Omega 2024, 9, 34507−34529

unexplored. Through the investigation of MO/LDH nanocomposites, our study aims to bridge this gap in the literature by providing valuable insights into the combined antibacterial properties of these materials. We anticipate that the unique physicochemical characteristics of MO/LDH nanocomposites, such as their size, charge, and composition, may lead to improved antimicrobial activity compared to that of their individual components. This exploration holds great promise for the development of advanced antibacterial agents that exhibit enhanced efficacy, reduced toxicity, and potential applications in addressing antibiotic-resistant bacterial strains. In summary, our research addresses the limited understanding of the antibacterial properties of MO/LDH nanocomposites. Our study seeks to contribute novel insights into the synergistic effects of these nanomaterials, providing innovative solutions for the fight against bacterial infections.

2. MATERIALS AND METHODS

2.1. Soil Sample Collection and Actinobacteria Isolation. The soil samples were collected from the eastern desert, Beni-Suef, Egypt. The soil samples were obtained aseptically at a depth of 15−20 cm from the rhizosphere of the dominant plants, such as *Zilla spinosa* and *Zygophyllum album*, with a collecting spatula in sterile plastic bags. Afterward, they were air-dried for 7 days at room temperature to reduce the population of vegetative bacterial cells. The isolation of Actinobacteria was performed by the serial dilution plate technique; approximately 1 g of soil sample was subjected to serial dilution until a dilution of 10^{-5}, after which approximately 100 μL of the diluted sample was spread on ISP-2 (International Streptomyces Project 2) isolation medium (10 g/L malt extract, 4 g/L yeast extract, 4 g/L glucose, and 20 g/L agar, and the final pH was adjusted to 7.2 ± 0.2). The ISP-2 plates were incubated at 30 °C for 14 days. Various colonies of Actinobacteria were subcultured until pure cultures were obtained, and then the isolates were stored as spore suspensions in glycerol (20%) at −80 °C for further experiments.

2.2. Characterization of Actinobacteria Isolate. *2.2.1. Morphological Characteristics.* The technique of coverslip culture, as described by Okami and Suzuki 1958,[80] was utilized to explore the morphological characteristics of our actinobacteria isolate on yeast extract-malt extract agar (ISP-2) media, as established by Pridham et al., 1957.[81] A trough was created by removing a strip of agar from the poured plates, with the margins of said trough being inoculated with the chosen actinobacterial strain. Sterile coverslips were then placed over the trough, and the plates were incubated at 28 °C for 7, 14, and 21 days. Once this incubation period had elapsed, the coverslips were removed along with any adhering growth, and the resulting coverslip cultures were subjected to microscopic examination and imaging using an electron microscope at an appropriate magnification. This approach was designed to facilitate a thorough analysis of the morphological features of the actinobacterial strains being studied.

2.2.2. Cultural Characteristics. The cultural features of the chosen actinobacteria isolate were examined on the following ISP media: tryptone-yeast extract medium (ISP-1), malt extract-yeast extract medium (ISP-2), oatmeal agar medium (ISP-3), inorganic salt-starch agar medium (ISP-4), glycerol-asparagine agar medium (ISP-5), and tyrosine agar (ISP-7).[82]

2.2.3. Biochemical and Physiological Characterization. 2.2.3.1. Utilization of Various Carbon Sources. The ability of the actinobacterial strains to employ various substances as the sole carbon sources for both energy and growth was evaluated through the use of the protocol proposed by Shirling and Gottlieb, 1966.[82] The basal medium composition (ISP-9)[83,84] is shown in Table 1.

Table 1. ISP-9 Medium Composition

ingredients	(G/Liter)
$(NH_4)_2SO_4$	2.64 g
K_2HPO_4	5.65 g
$MgSO_4{\cdot}7H_2O$	1 g
KH_2PO4	2.38 g
trace salts solution	1 mL
agar	15 g
final pH	7.2 ± 0.2

The trace salt solution is composed of a variety of components, including $CuSO_4{\cdot}5H_2O$, $FeSO_4{\cdot}7H_2O$, $MnCl_2{\cdot}4H_2O$, $ZnSO_4{\cdot}7H_2O$, and distilled water, each in precise amounts of 0.64 g, 0.11 g, 0.79 g, 0.15 g, and 100 mL, respectively.

The carbon sources employed in this study include a range of monosaccharides, disaccharides, and polysaccharides, including D-glucose, D-xylose, D-mannitol, D-fructose, D-galactose, D-lactose, D-mannose, maltose, sucrose, and starch.

2.2.3.2. Enzymes and Related Biochemical Tests. The amylolytic activity and catalase activity of the actinobacterial strain studied were evaluated using modified Bennett's agar (MBA) media, as proposed by Jones, 1949.[85] Lipase activity can be demonstrated by the technique of Sierra, 1957.[86]

2.2.3.3. Physiological Characterization. The growth capacity of the test strain was evaluated on MBA media at different temperatures ranging from 4 to 45 °C, different concentrations of sodium chloride (1, 2, 3, 4, 5, 6, 7, 8, 9, 10, 11 and 12% w/v), and various pH values ranging from 3 to 10.

2.2.4. Molecular Studies. 2.2.4.1. DNA Preparation, Amplification, and 16S rDNA Gene Sequencing. Chromosomal DNA was extracted and amplified following the methodology employed by Kim et al., 2000.[87] Subsequently, the amplified products were separated via gel electrophoresis. This separated preparation was then purified using a Nucleospin Extraction Kit manufactured by Biogen Ltd. and subjected to direct sequencing. Direct sequencing was performed using a Taq DyeDeoxy Terminator Cycle Sequencing Kit produced by Applied Biosystems and oligonucleotide primers as previously described by Chun and Goodfellow, 1995.[88] Then, gel electrophoresis was performed to determine the sequence of the nucleotide sequences. This was accomplished by employing an Applied Biosystems DNA sequencer (model 373A) and the accompanying software provided by the manufacturer.

2.2.4.2. Phylogenetic Analysis. Alignments were performed between almost all the full-length 16S rRNA gene sequences and the reference sequences obtained from EzBioCloud utilizing CLUSTAL W.[89] The resulting 16S rRNA sequences were examined and matched for sequence similarity with those of EzBioCloud.[90] Then, the phylogenetic tree was developed using MEGA 11 software with confidence checking through the bootstrap value of 1000 repeats.

2.3. Preparation of Cell-Free Supernatant. Actinobacterial strains were inoculated on ISP-2 agar media for 7 days at 28 °C. A loopful of well-grown culture was then inoculated in 20 mL of ISP-2 broth medium within a 100 mL Erlenmeyer flask and incubated for 2 days at 28 °C at 150 rpm in

https://doi.org/10.1021/acsomega.4c02133
ACS Omega 2024, 9, 34507−34529

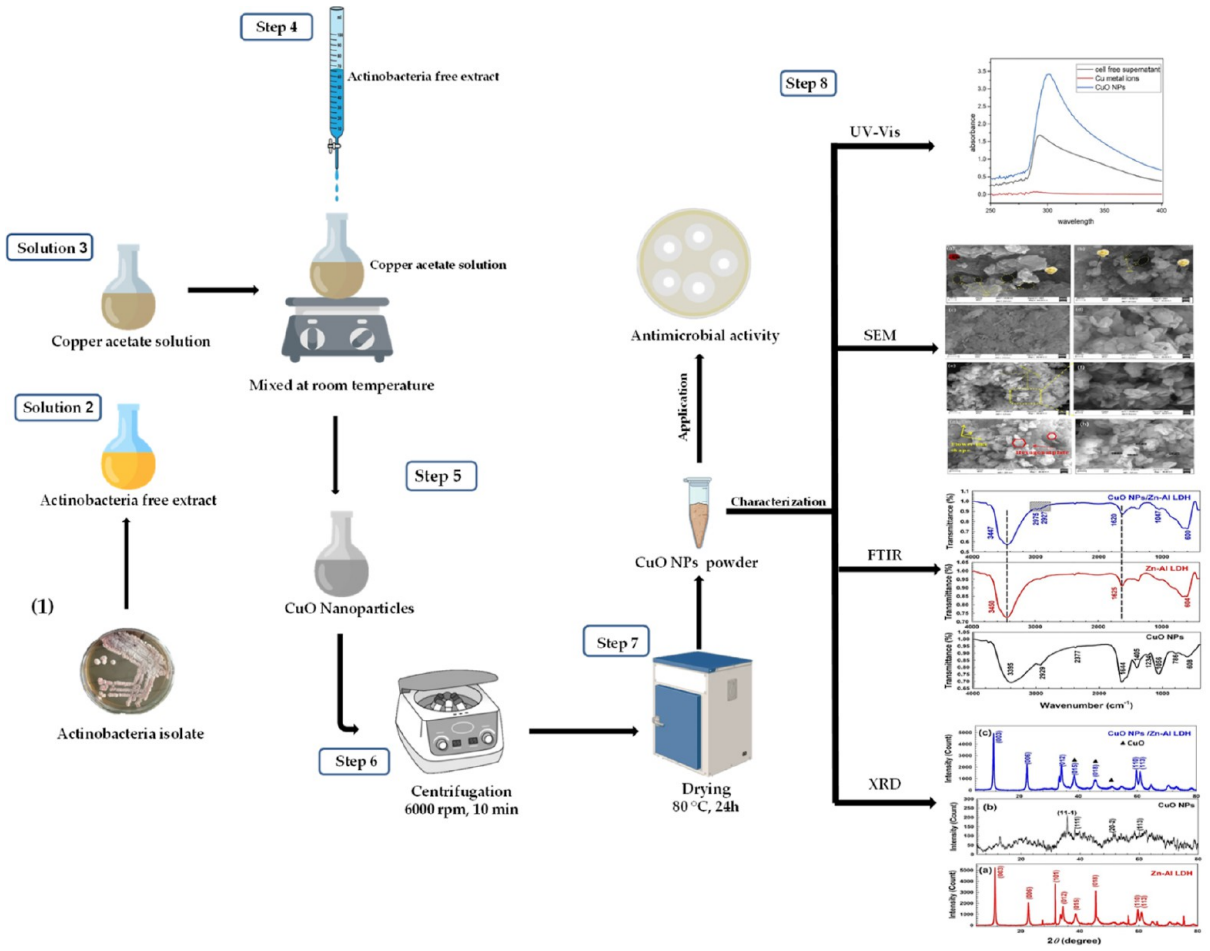

Figure 1. Schematic representation of the actinobacteria-mediated synthesis of CuO flower-like structures.

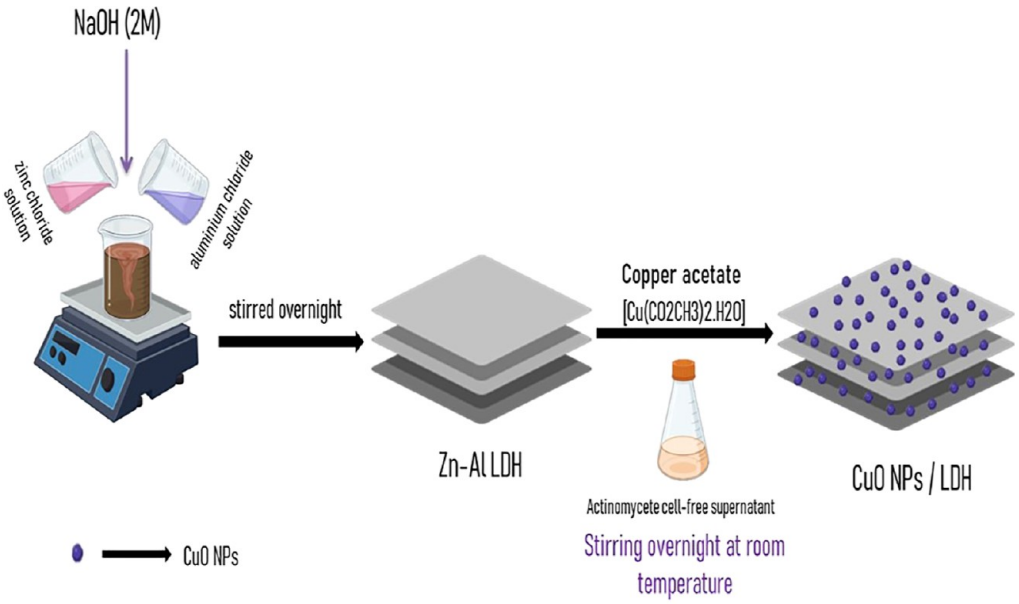

Figure 2. Schematic representation of the CuO NPs/Zn−Al LDH synthesis procedure.

a shaker incubator. After growth, the prepared inoculum was transferred to a freshly prepared medium within a 500 mL flask and then kept in a shaker incubator at 30 °C for 7 days at 150 rpm. After incubation, the culture was subjected to centrifugation at 6000 rpm for 10 min to clear the supernatant from the actinobacteria cells.

2.4. CuO Nanoparticles Biosynthesis. The steps for CuO biosynthesis are illustrated in Figure 1. As shown, cells from the actinobacteria culture (1) were separated, and a cell-free extract

https://doi.org/10.1021/acsomega.4c02133
ACS Omega 2024, 9, 34507−34529

solution was prepared (solution 2). An equivalent of 10 mM of a solution of copper acetate [Cu $(COOCH_3)_2{\cdot}H_2O$] (solution 3) was prepared next. The supernatant cell-free extract solution was introduced dropwise to the copper acetate aqueous solution under continuous stirring (step 4), and the mixture was kept at room temperature for 24 h using a shaker. The bioreduction of Cu metal ions and the formation of CuO nanoparticles due to a color change (step 5) were detected using a UV−vis spectrophotometer. The synthesized CuO NPs were collected via centrifugation for 10 min at 6000 rpm (step 6) and then washed several times in deionized water. Then, the CuO NPs were dried at 80 °C and stored for later use (step 7). The prepared samples were characterized using several techniques, as described in the next subsection (step 8).

2.5. Zn−Al LDH Synthesis. Using the coprecipitation method, Zn−Al LDH (4:1 M ratio) was produced. Energy-dispersive X-ray spectroscopy was used, however, to examine the chemical composition of the organized Zn−Al LDH. After mixing the zinc chloride solution and aluminum chloride salts, 100 mL of deionized water were dissolved at room temperature (25 °C) while stirring continuously. A sudden increase in pH that could lead to the formation of carbonate-containing LDH was avoided, and the mixture was not heated to 80 °C when the base was added by gradually blending in a sodium hydroxide solution (2 mol/L) until the precipitate was fully blended and pH 9 was reached.[91] The system was vigorously shaken for an additional twenty-4 h at room temperature (25 °C). After that, the system was repeatedly cleaned and filtered using distilled water and then treated with ethanol until the pH reached 7 to partially remove the carbonaceous products that had adsorbed.[92] The resultant precipitate was dried in a vacuum oven for 24 h at 60 °C.[93] After that, the Zn−Al LDH was ground to a uniform particle size.

2.6. Preparation of CuO NPs/Zn−Al LDH Nanocomposite. First, 2 g of LDH was suspended in 100 mL of aqueous copper acetate and stirred continuously for 24 h. Then, the cell-free supernatant of an Actinobacteria isolate was added dropwise to the previous suspension, which was aged overnight, under continuous stirring. Finally, the precipitate was centrifuged and washed with distilled water, and the collected powder was dried at 80 °C for 24 h. These steps are schematically illustrated in Figure 2.

2.7. Characterization of Synthesized Nanomaterials. A UV−vis spectrophotometer with a wavelength ranging from 200 to 800 nm was used to track the biosynthesis of CuO nanoparticles. Moreover, the XRD patterns were collected using an X-ray diffractometer (Panalytical Empyrean) operating at 40 kV with a current of 35 mA and Cu Ka radiation (wavelength of 0.154 nm), and the (2θ) scanning rate was 5 to 80° at 8 min^{-1}. In addition, the biomolecules and functional groups of the samples were identified using a Fourier transform infrared (FTIR) spectrometer (Bruker-Vertex, Germany) with a wavenumber range of 400−4000 cm^{-1}. Field emission scanning electron microscopy was used to investigate the morphology and particle size of the synthesized nanomaterials. Zeta potential and hydrodynamic particle size measurements were conducted using a Zetasizer Nano (Malvern Instruments Ltd.).

2.8. Estimation of the Antimicrobial Activity of CuO NPs, Zn−Al LDH, and CuO/Zn−Al LDH Nanocomposite.

2.8.1. Culture Media. To evaluate the biological efficacy of the CuO NPs, Zn−Al LDH, and CuO NPs/Zn−Al LDH nanocomposite, the culture media of Nutrient Broth and Nutrient agar were procured from HiMedia Laboratories (Mumbai, India). These culture media were subsequently prepared and used for bacterial growth following the guidelines provided by the manufacturers.

2.8.2. Bacterial and Fungal Strains. All bacterial strains, including methicillin-resistant *S. aureus* ATCC 43300, *Listeria monocytogenes* ATCC 7644, (a Gram-positive bacterium), *Salmonella typhimurium* ATCC 14028, *Pseudomonas aeruginosa* ATCC 9027 (a Gram-negative bacterium), and the fungal strain *Candida albicans* ATCC 60913, were obtained from the microbial culture collection of the Department of Botany and Microbiology, Faculty of Science, Beni-Suef University, Beni-Suef, Egypt.

2.8.3. Inoculum Preparation. The suspensions were carefully prepared from recently cultivated cultures. First, the cultures were plated on nutrient agar and incubated at 37 °C for 24 h. After the incubation period, approximately 1−2 colonies were transferred to test tubes containing 5 mL of 0.9% saline solution using a sterile loop. The suspensions were then vigorously stirred for 15 s using a vortex apparatus to ensure thorough mixing. Then, the turbidity of the final inoculum was standardized. This was achieved by using a carefully measured barium sulfate suspension with a value of 0.5 on the McFarland scale. The resulting standardized inoculum had a final concentration of approximately 1.5×10^8 colony-forming units per milliliter (cfu/mL).

2.8.4. Agar-Well Diffusion Technique. The antimicrobial properties of CuO NPs, Zn−Al LDH, and the CuO NPs/Zn−Al LDH nanocomposite were evaluated for their effectiveness against a variety of microorganisms, including methicillin-resistant *S. aureus* ATCC 43300, *L. monocytogenes* ATCC 7644, (a Gram-positive bacterium), *S. typhimurium* ATCC 14028, *P. aeruginosa* ATCC 9027 (a Gram-negative bacterium), and the fungal strain *C. albicans* ATCC 60913. To assess the antimicrobial activity of our samples against the bacterial isolates, the agar-well diffusion technique was employed by creating 6 mm-diameter wells in an agar plate using a sterile plastic pipet. To carry out this technique, a bacterial culture with a concentration of 0.5 McFarland was inoculated onto nutrient agar plates using the pour plate method. Next, the wells were filled with 100 μL of the tested sample, which was prepared at various concentrations (0.125, 0.25, 0.5, 1, and 5 mg/mL) and allowed to incubate at room temperature for 2 h. Subsequently, the plates were incubated at 37 °C for 24 h. After the incubation period, the inhibition zones resulting from the antimicrobial activity of the samples were carefully observed and recorded in mm.

2.8.5. Minimum Inhibitory Concentration Determination. The determination of the minimum inhibitory concentration (MIC) was performed utilizing a modified dilution technique. In this particular approach, sterile nutrient broth was used to dilute the generated nanomaterials (CuO NPs, Zn−Al LDH, and CuO NPs/Zn−Al LDH nanocomposite) to various concentrations ranging from 7.8 to 250 μg/mL in test tubes. Subsequently, approximately 10 μL of methicillin-resistant *S. aureus* ATCC 43300 culture and 0.5 McFarland standard were introduced into test tubes containing 1 mL of prepared sample concentrations in nutrient broth. The same procedure was applied to *S. typhimurium* ATCC 14028, *L. monocytogenes* ATCC 7644, *P. aeruginosa* ATCC 9027, and *C. albicans* ATCC 60913. Next, the tubes were incubated at 37 °C for 18 to 24 h and observed for any indications of growth or turbidity. The MIC was identified as the lowest concentration of the tested substance that demonstrated observable inhibition of bacterial growth.

https://doi.org/10.1021/acsomega.4c02133
ACS Omega 2024, 9, 34507−34529

2.8.6. Kill-Time Curve of the CuO NPs, Zn−Al LDH, and CuO NPs/Zn−Al LDH Nanocomposite. Time−kill curve assays were conducted to confirm the microbicidal activity of the CuO NPs, Zn−Al LDH, and CuO NPs/Zn−Al LDH nanocomposite against *S. aureus and C. albicans*. In this study, *S. aureus* and *C. albicans* cells were cultured in Mueller−Hinton broth at 28 °C for 24 h. The cells were then centrifuged, washed, and resuspended at a concentration of 2.5×10^5 cells/mL, with the addition of CuO NPs, Zn−Al LDH, or CuO NPs/Zn−Al LDH at a concentration equivalent to their MICs. The mixtures were incubated at 28 °C, and 50 μL aliquots were taken at specific time intervals (0, 1, 2, 4, 6, and 24 h). Serial dilutions were performed, and 50 μL from each dilution was spread onto tryptic soy agar plates, which were then incubated at 37 °C for 48 h to determine the number of colony-forming units (cfus) per mL.

2.8.7. Effect of the Synthesized CuO NPs, Zn−Al LDH, and CuO NPs/Zn-AL LDH on Bacterial Protein Leakage. A mature bacterial culture of 18 h was adjusted to a 0.5 McFarland standard, equivalent to 1.5×10^8 colony-forming units per milliliter (cfu/mL). Then, 100 μL of this culture was introduced into 10 mL of nutrient broth containing well-dispersed CuO NPs, Zn−Al LDH, and CuO NPs/Zn-AL nanocomposite at varying concentrations (0.125, 0.25, 0.5, and 1.0 mg/mL). Nutrient broth without nanocomposites inoculated with the culture served as the control group. Following treatment, the samples were incubated at 37 °C for 5 h and then centrifuged at 6000 rpm for 20 min. From each sample, 100 μL of the supernatant was mixed with 1 mL of Bradford reagent. The optical density of these mixtures was determined at 595 nm after allowing them to sit in the dark for 10 min[94]

2.8.8. Transmission Electron Microscopy Analysis of S. aureus Bacteria Treated with CuO NPs, Zn−Al LDH, and the CuO NPs/Zn−Al Nanocomposite. The structural changes in *S. aureus* treated with 2× MIC of synthesized CuO NPs, Zn−Al LDH, and CuO NPs/Zn−Al LDH nanocomposite at 37 °C for 24 h were analyzed using Transmission Electron Microscopy (TEM). Bacterial cells were isolated from 24 h-old cultures in nutrient broth by centrifugation at 4000 rpm for 10 min and then washed with distilled water. The samples were then fixed in a 3% solution of glutaraldehyde, washed with PBS, and further fixed with a potassium permanganate solution for 5 min at ambient temperature. Following fixation, the samples underwent a dehydration process using an ethanol gradient from 10 to 90% for 15 min in each concentration of ethanol and finally in absolute ethanol for 30 min. The samples were then gradually infiltrated with a mixture of epoxy resin and acetone, ending in pure resin. Ultrathin sections were prepared on copper grids, which were subsequently stained with uranyl acetate and lead citrate. The stained sections were examined using a JEOL-JEM 1010 transmission electron microscope at 70 kV at The Regional Center for Mycology and Biotechnology, Al-Azhar University.

3. RESULTS AND DISCUSSION

3.1. Isolation and Identification of Actinobacteria Isolate. A total of 49 Actinobacteria were obtained from the collected soil samples. All the Actinobacteria isolates were examined for their ability to synthesize CuO NPs. One of the isolated actinobacteria, ISP-2 27, showed the most promising findings with the highest optical density. Therefore, we utilized it for the remainder of the study. Morphological characteristics revealed that the ISP-2 27 strain was able to produce good and branched substrate hyphae when cultured on ISP-2 medium.

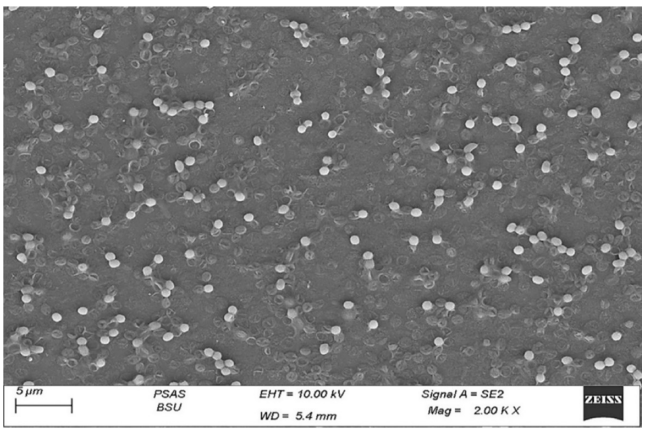

Figure 3. SEM image of the actinobacteria isolate ISP-2 27.

Table 2. Cultural Characteristics of the ISP-2 27 Isolate

medium	character	ISP-2 27
ISP-1	growth	moderate
	aerial mycelium	greenish gray
	substrate mycelium	olive dark
	soluble pigments	none
ISP-2	growth	abundant
	aerial mycelium	dark green
	substrate mycelium	dark green
	soluble pigments	none
ISP-3	growth	weak
	aerial mycelium	light yellow
	substrate mycelium	pale yellow
	soluble pigments	none
ISP-4	growth	moderate
	aerial mycelium	pale green
	substrate mycelium	blackish green
	soluble pigments	none
ISP-5	growth	weak
	aerial mycelium	pale yellow
	substrate mycelium	pale yellow
	soluble pigments	none
ISP-7	growth	weak
	aerial mycelium	dark grayish brown
	substrate mycelium	brownish black
	soluble pigments	none

Table 3. Utilization of Various Carbon Sources by the Selected Actinobacterial Strain (ISP-2 27)[a]

Carbon source	ISP-27
D-glucose	++
D-xylose	+
D-mannitol	±
D-fructose	++
D-galactose	+
D-lactose	++
D-mannose	−
maltose	+
sucrose	+
starch	++

[a]++ Good utilization, + moderate utilization, ± Weak or doubtful utilization, − No utilization.

https://doi.org/10.1021/acsomega.4c02133
ACS Omega 2024, 9, 34507−34529

Table 4. Physiological and Biochemical Characterization of the Selected Actinobacterial Strain[a]

characteristic	ISP-2 27
Biochemical Tests	
amylase test	+
catalase test	+
lipase test	+
Effect of Temperature	
4 °C	−
10 °C	−
15 °C	−
20 °C	+
25 °C	+
30 °C	+
35 °C	+
40 °C	+
45 °C	±
Effect of Salinity (NaCl)	
2%	+
5%	+
7%	−
10%	−
12%	−
Growth at Different pH	
3	−
4	+
5	+
6	+
7	+
8	+
9	+
10	+

[a]+: Growth, ±: Weak or doubtful growth, −: No growth.

Moreover, the nonmotile and oval spores were observed to be borne singularly on the substrate mycelium. The spore surface was found to be smooth in texture, as shown in Figure 3.

3.2. Cultural Characteristics. Table 2 displays the culture characteristics of the actinobacterial strain ISP-2 27, which was chosen for this study. Strain ISP-2 27 exhibited weak growth on ISP-3, ISP-5, and ISP-7 media, moderate growth on ISP-1 and ISP-4 media, and abundant growth on ISP-2 media, wherein the aerial mycelium ranged in color from pale yellow to dark grayish brown, while the substrate mycelium varied in color from pale yellow to black. No soluble pigments were detected on any of the utilized media.

3.3. Biochemical and Physiological Characterization. *3.3.1. Carbon Source Utilization.* Table 3 presents the utilization of carbon sources by the selected actinobacteria isolate for this study. Our strain exhibited good to moderate growth when provided with D-glucose, D-xylose, D-fructose, D-galactose, D-lactose, maltose, sucrose, and starch as the sole carbon sources for both growth and energy production but exhibited weak or no growth on D-mannitol and D-mannose, respectively.

3.3.2. Enzymes and Physiological Characterization. Table 4 presents a comprehensive overview of the physiological and biochemical characteristics of the tested actinobacterial strain. The data clearly showed that the tested strain exhibited remarkable amylase, catalase, and lipase enzyme production. The tested actinobacterial strain showed good growth between 20 and 40 °C, with the optimal temperature being approximately 30 °C. Additionally, our isolate showed good growth when exposed to NaCl concentrations of up to 5%. Furthermore, the isolate exhibited good growth rates when exposed to a wide range of pH conditions, specifically between 6 and 10. However, it is important to note that our isolate displayed exceptional abilities to thrive at a lower pH until it reached pH 4.

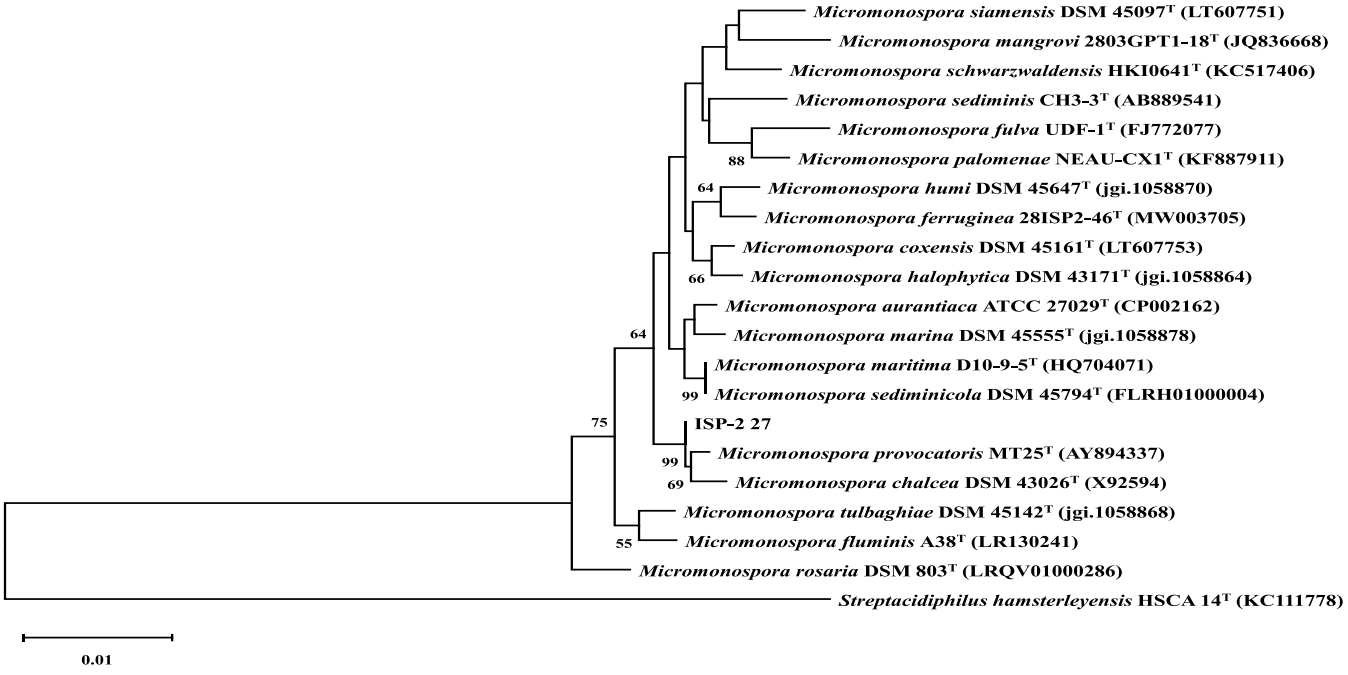

Figure 4. Relationships between the ISP-2 27 strain and closely associated species of the genus *Micromonospora* in a neighbor-joining tree based on nearly complete 16S rRNA gene sequences. The numbers at the nodes represent the percentages of the bootstrap levels based on 1000 resampled data sets. Only percentages greater than 50% are provided. Bar = 0.01 substitutions for each positional nucleotide. *Streptacidiphilus hamsterleyensis* HSCA14^T (KC111778) was used to estimate the root position of the tree.

https://doi.org/10.1021/acsomega.4c02133
ACS Omega 2024, 9, 34507−34529

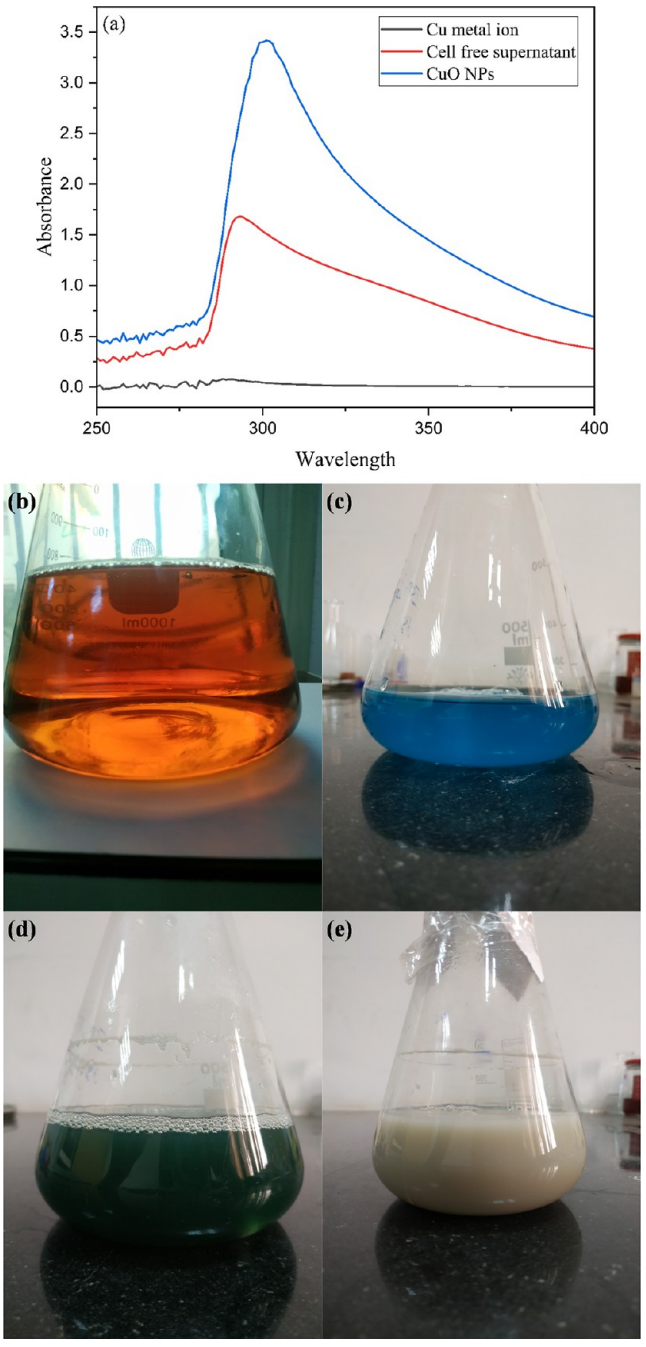

Figure 5. (a) UV−vis spectra of the CuO NPs biosynthesized from actinobacteria isolate cell-free supernatant, (b) actinobacteria-free extract, (c) copper metal ions solution, (d) copper oxide nanoparticles, and (e) CuO NPs/Zn−Al LDH nanocomposite.

3.4. Molecular Studies. Nearly complete 16S rRNA sequences were obtained for the actinobacteria isolate ISP-2 27. A preliminary examination was conducted to compare the 16S rRNA sequence of strain ISP-2 27 with those available in the EzBioCloud database, revealing that it belongs to the genus *Micromonospora*. The phylogenetic tree shown in Figure 4 represents the relationship between strain ISP-2 27 and other *Micromonospora* species. Furthermore, based on phylogenetic tree analysis, the Actinobacteria isolate ISP-2 27 was found to be closely associated with the type strain of *Micromonospora provocatoris* MT25^T, with a bootstrap value of 99% in the neighbor-joining tree, as shown in Figure 4.

3.5. Characterization of the Prepared Nanomaterials. Biosynthesized CuO nanoparticles (NPs) were primarily confirmed through visual observation of a significant color change from blue to green. This transformation occurred when a 10 mM solution of copper acetate was introduced to the cell-free supernatant of the actinobacteria isolate. The alteration in color can be attributed to the excitation of surface plasmon resonance (SPR) effect,[95] as well as the bioreduction of copper acetate [$Cu(CO_2CH_3)_2{\cdot}H_2O$]. In contrast, when aqueous copper acetate was incubated under the exact conditions without the addition of the cell-free supernatant, no change was detected. Subsequently, the presence of nanomaterials was verified using UV−visible spectrophotometry, which allowed for analysis within a wavelength range of 200−800 nm. Within this analysis, the absorption peak of CuO NPs was identified between 290 and 330 nm, indicating that CuO NPs were successfully produced, as illustrated in Figure 5. Furthermore, the UV−vis spectrum of the biosynthesized CuO NPs displayed an optimum peak at 300 nm, which was directly associated with the shift in SPR. Additionally, based on the phenomenon of interband switching, which refers to the transition of copper metal core electrons from one energy band to another, it can be observed that CuO NPs exhibit a distinct peak. This peak arises due to the aforementioned interband switching of the electrons within the metal core of copper, confirming that CuO NPs were formed.[96] Similar absorbance peaks were reported for CuO nanoparticles in the open literature.[97,98]

The exact mechanisms by which microorganisms such as actinobacteria, fungi, and yeast produce nanoparticles are still being studied; however, their synthesis involves extracellular and intracellular pathways in which enzymes have a significant impact, contributing to the overall mechanism of nanoparticle production.[99,100] The possible mechanism involved in the bioreduction, capping, and stabilization of Cu^{2+} into metallic form is promoted by the presence of enzymes, proteins, peptides, reducing cofactors, phytochemicals, and organic materials found in the cell wall or released from the cell into the growth media.[101,102] An illustration of the proposed mechanism involved in the production of CuO nanoparticles utilizing the cell-free extract of the actinobacteria isolate ISP-2 27 is shown in Figure 6.

The X-ray diffraction patterns of the CuO nanoparticles, Zn−Al LDH, and CuO NPs/Zn−Al LDH nanocomposite are shown in Figure 7. Figure 7a shows typical XRD diffraction patterns of the LDH material. As shown, the sharpness of the diffraction peaks in the Zn−Al LDH XRD pattern illustrates its high crystallinity.[103] The peaks at 2 theta angles of 11.26 and 22.57° can be attributed to the basal plane peaks (003) and (006), respectively. On the other hand, the peaks at 31.7, 34.27, 38.64, 45.4, 59.67, and 60.91° can be attributed to the nonbasal plane peaks (101), (015), (018), (012), (110) and (113), respectively.[104] XRD analysis of the biosynthesized CuO NPs is presented in Figure 7b. The diffraction peaks at 2θ values of 35.5, 38.4, and 58.3° can be attributed to the (002), (111), and (202) planes, respectively, which are consistent with those of the monoclinic phase of CuO (JCPDS 45-0937). These results match the findings of other researchers who reported the monoclinic phase of CuO.[96,105] As shown, CuO is formed in an amorphous structure, probably due to the biosynthesis procedure that lacks control over the long-range order of the crystallized oxide. For the nanocomposite, both phases had common peaks, as illustrated in Figure 7, but no distinct peaks for the CuO phase could be observed, and the peaks of the LDH

https://doi.org/10.1021/acsomega.4c02133
ACS Omega 2024, 9, 34507−34529

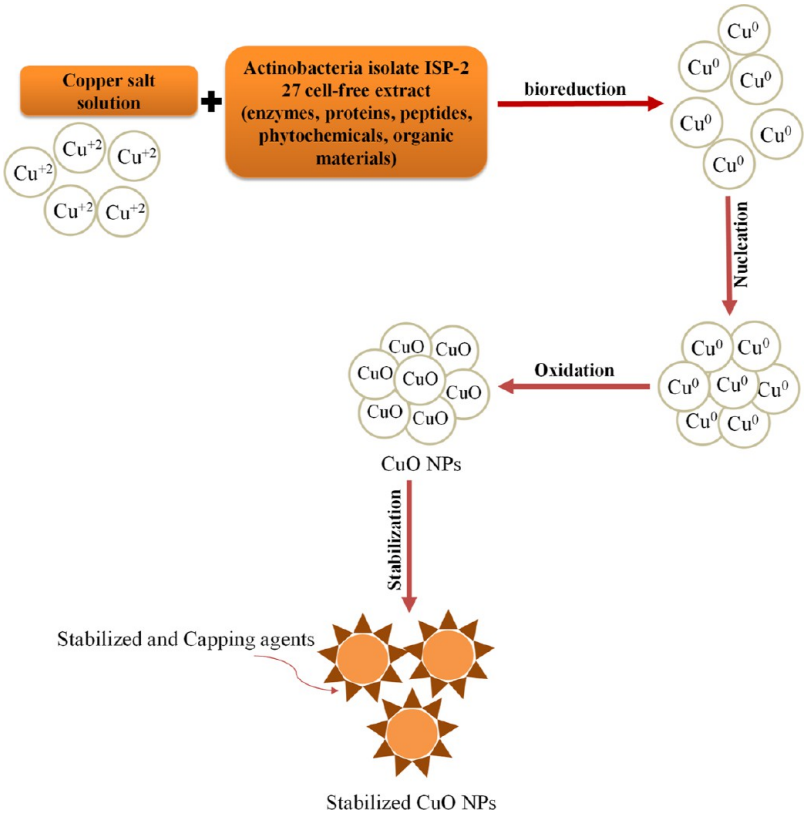

Figure 6. Proposed mechanism involved in the production of CuO nanoparticles utilizing the cell-free extract of the actinobacteria isolate ISP-2 27.

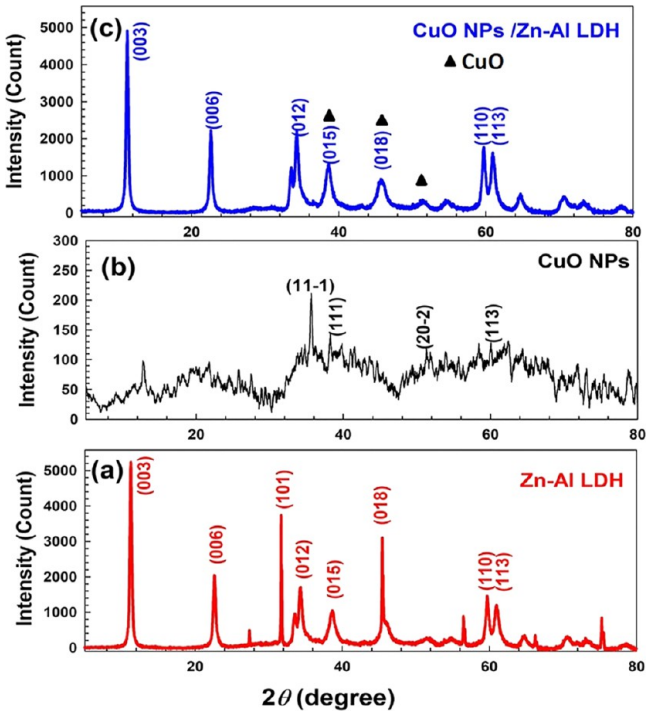

Figure 7. XRD patterns of the (a) Zn−Al LDH, (b) CuO NPs, and (c) CuO NPs/Zn−Al LDH nanocomposite.

phase were dominant. This may be due to the amorphous nature of the CuO phase in the composite. The average crystallite size was calculated using the Debye−Scherrer equation (eq 1).[106]

$$D = K\lambda/\beta \cos\theta \quad (1)$$

$$\text{strain} = \beta\cos\theta/4 \quad (2)$$

Here, D is the nanocomposite crystallite's size, k represents the lattice constant, (0.9), λ is the X-ray wavelength of the Cu Kα radiation (0.15406 nm), and β refers to the full width at half-maximum and indicates the incident angle. The average crystallite sizes calculated for CuO NPs, LDH, and CuO NPs/Zn−Al LDH, according to eq 1, were 17.43, 2.01243, and 2.76147 nm, respectively. The strains were 0.00329, 0.012132, and 0.012696 for CuO NPs, LDH, and CuO NPs/Zn−Al LDH, respectively. From the results, we conclude that the changes in the crystallite size and strain confirm the loading of CuO on LDH.

Concerning LDH, the average distance between cation−cation interactions in the brucite-like layer can be determined by using the lattice parameter "a", which is calculated using the equation: $a = 2d\ (110)$. This lattice parameter provides important insights into the structural arrangement of the material. Additionally, the lattice parameter "c" indicates the thickness of the films and can be calculated as $c = 3d\ (003)$. Specifically, the lattice parameters "a" and "c" for LDH have been determined to be 0.3084 and 2.3026 nm, respectively. These lattice parameters agree well with those reported for hydrotalcite-like compounds.[107]

The morphology of the prepared nanomaterials is illustrated in the SEM images presented in Figure 8. The SEM micrographs of the biosynthesized CuO NPs revealed a flower-like morphology with high porosity, as shown in Figure 8a,b. The SEM images of Zn−Al LDH revealed a traditional hexagonal plate-like morphology arranged in a lamellar structure, as shown in Figure 8c,d, which is characteristic of LDH materials.[103,108] The SEM micrographs in Figure 8e of the CuO NPs/Zn−Al LDH nanocomposite show both the flower-like structure of the

https://doi.org/10.1021/acsomega.4c02133
ACS Omega 2024, 9, 34507−34529

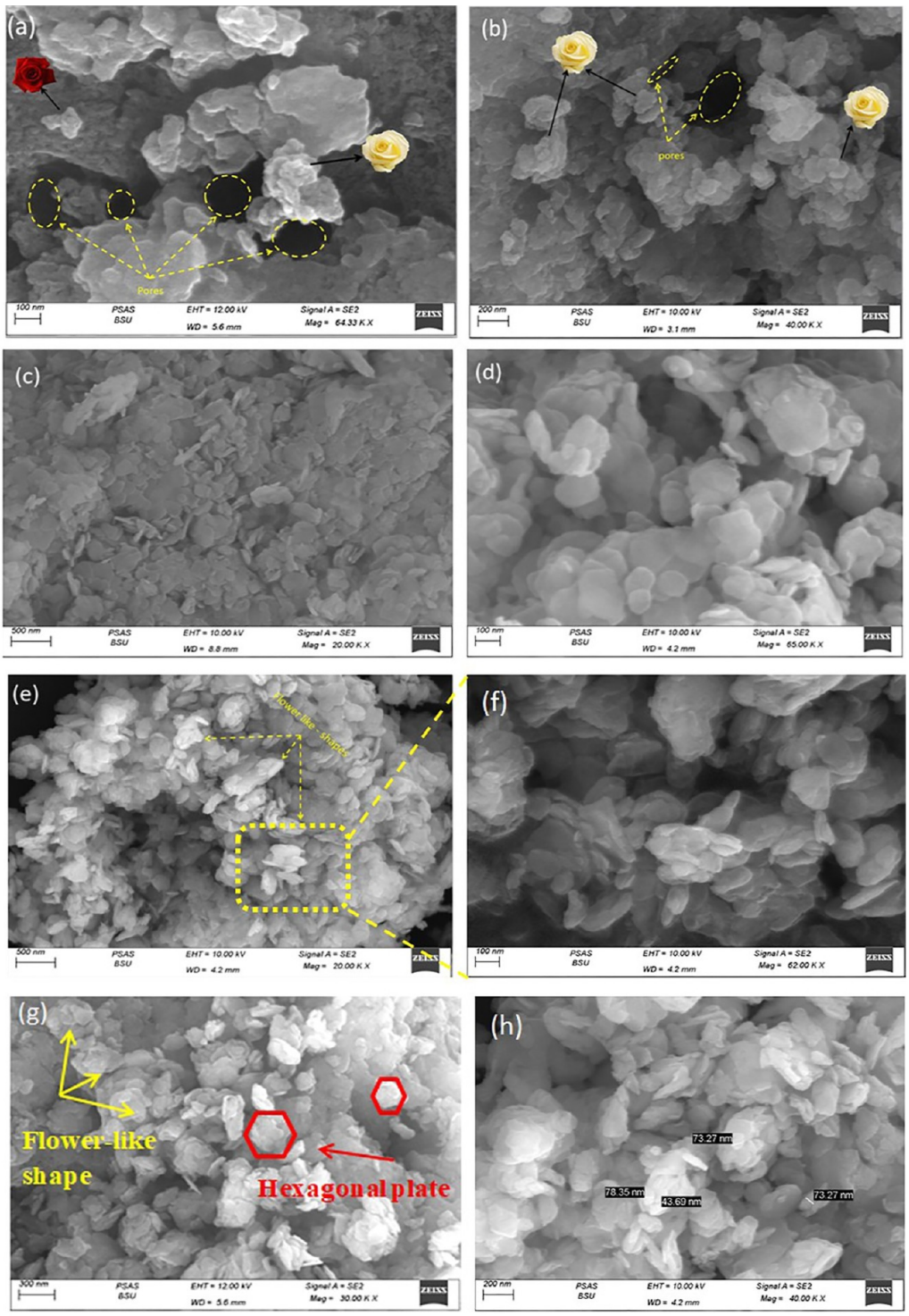

Figure 8. SEM images of (a,b) CuO NPs, (c,d) ZnAl LDH, and (e,h) CuO NPs/LDH nanocomposite. (f) Magnified image of the area shown in (e,g) an illustrative image of (e).

biosynthesized CuO NPs and the plate-like structure of Zn−Al LDH, which provided clear evidence of the loading of CuO NPs onto the LDH surface. The aggregated LDH plates can be clearly observed in the magnified image presented in Figure 8f, while the flower-like CuO phase is illustrated in Figure 8g. The size of the synthesized CuO phase in the nanocomposite ranged from 43 to 78 nm, as shown in Figure 8h.

EDX spectroscopy was performed to investigate the elemental composition of all the prepared materials. The EDX results of the CuO NPs, ZnAl LDH, and CuO NPs/LDH nanocomposites are shown in Figure 9a−c, respectively. As shown in Figure 9a, the pure signals for Cu indicate only the purity of the prepared sample with no foreign elements present. The C signal can originate from the background holder and/or from the carbonaceous compounds and biomolecules attached to the CuO surface from the biosynthesis process. Similarly, Figure 9b shows that the ZnAl LDH phase was formed with high purity

https://doi.org/10.1021/acsomega.4c02133
ACS Omega 2024, 9, 34507−34529

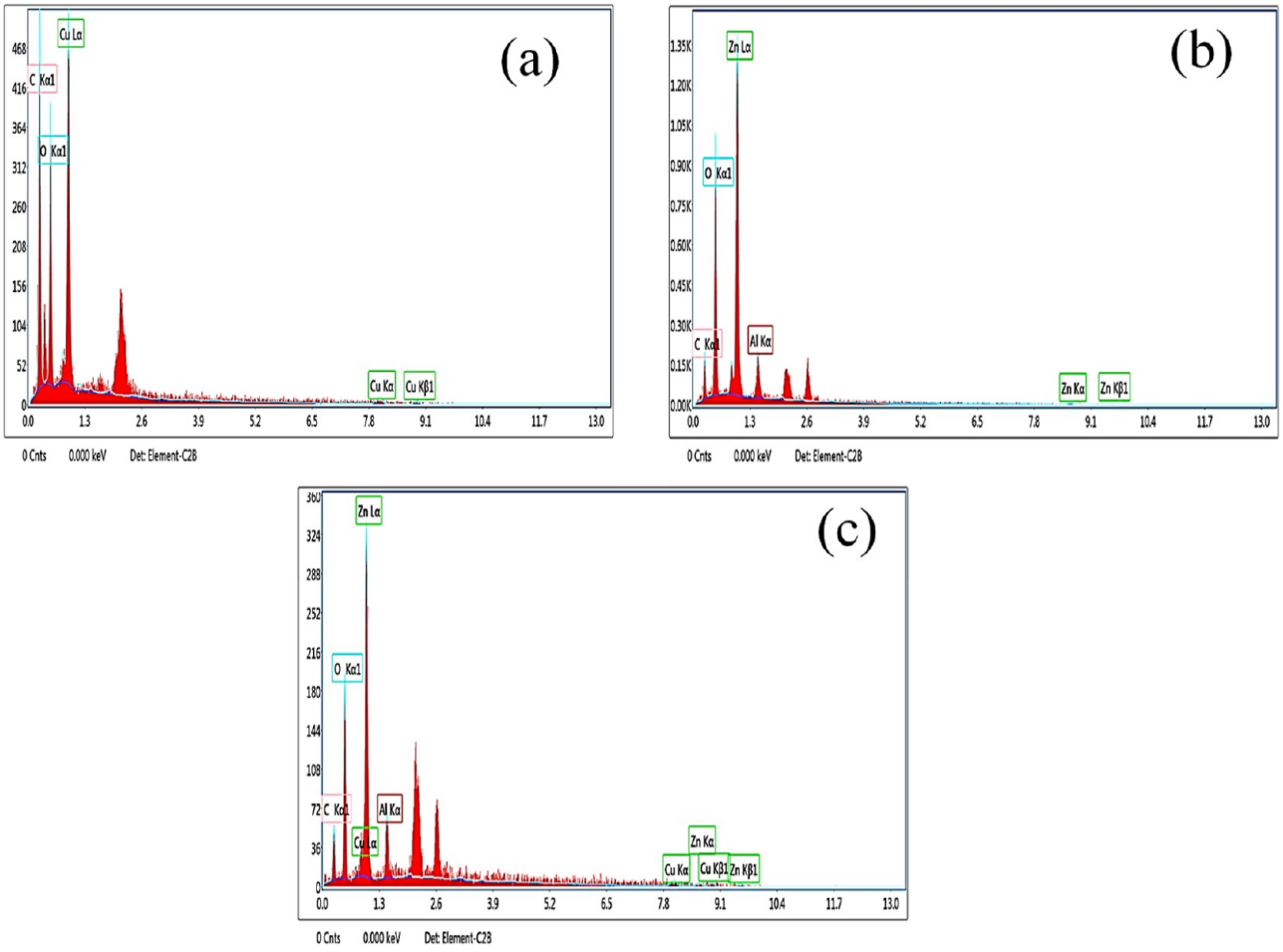

Figure 9. EDX spectra of the (a) CuO NPs, (b) Zn−Al LDH, and (c) CuO NPs/LDH.

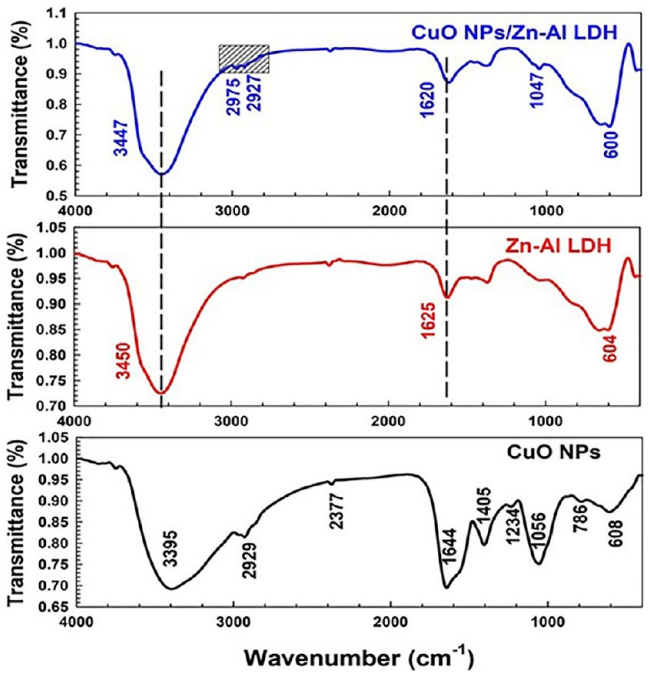

Figure 10. FTIR spectra of the CuO NPs, Zn−Al LDH, and CuO NPs/LDH nanocomposite.

with no signals for any other foreign elements. This is also true for the nanocomposite, as shown in Figure 9c.

The FTIR spectra of all the prepared nanomaterials are presented in Figure 10. For the biosynthesized CuO phase, the broadband at 3395 cm^{-1} could be attributed to OH stretching in adsorbed water molecules, alcohols, and phenols present in the bacterial media that were attached to the CuO surface. The peaks at 2929 and 2377 cm^{-1} were assigned to the stretching vibrations of C−H in alkanes and C≡C stretching of alkyne or CO_2 peak adsorbed onto protein molecules, respectively.[109,110] The peak observed at 1405 cm^{-1} indicates the presence of the O−H bending mode characteristic of carboxylic acid.[110] Furthermore, the band at 1644 cm^{-1} represents the C═O stretching of the amide I band of proteins.[111] The peaks observed at 1056 and 1234 cm^{-1} were related to the C−N stretching modes of amines. The presence of the monoclinic phase of the CuO NPs is supported by the peak at 608 cm^{-1}, which can be attributed to the metal−oxygen vibration (Cu−O).[110,112] All these peaks indicate the presence of several molecules, including proteins, which are essential for the stability, capping, and reduction of the produced CuO phase.

For LDH, the broad broadband at 3450 cm^{-1} is attributable to hydrogen bond stretching vibrations in the O−H group of interlayer molecules of water.[113] Moreover, the peak at 1625 cm^{-1} is related to the stretching vibration of H_2O molecules between layers. The peak that appeared at 1370 cm^{-1} could be attributed to the symmetric and asymmetric stretching of the C−O in the carbonate group $(CO_3)^{2-}$ that was produced during

https://doi.org/10.1021/acsomega.4c02133
ACS Omega 2024, 9, 34507−34529

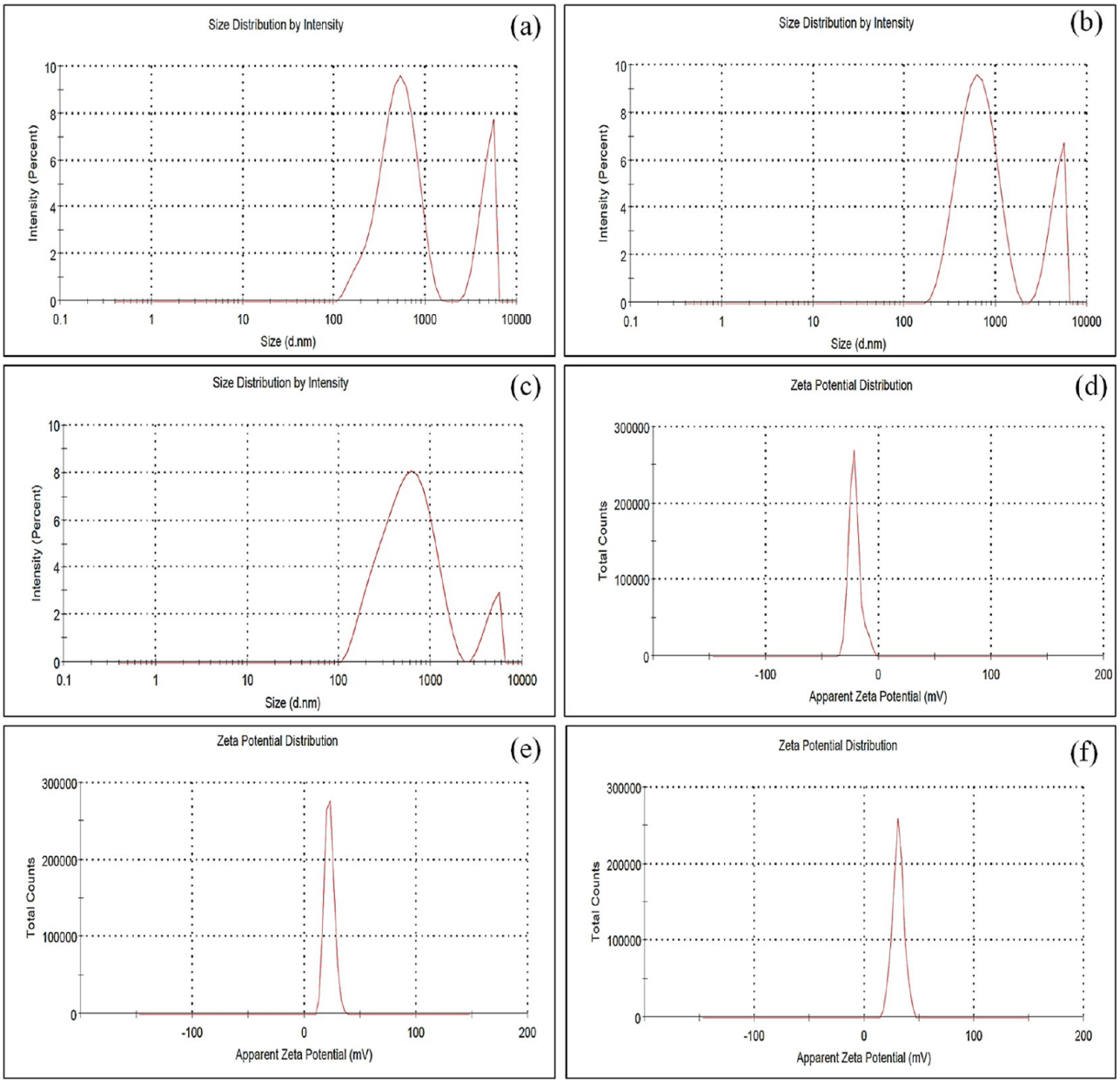

Figure 11. Hydrodynamic sizes of the (a) CuO NPs, (b) Zn−Al LDH, and (c) CuO NPs/LDH nanocomposite; and the zeta potentials of the (d) CuO NPs, (e) Zn−Al LDH, and (f) CuO NPs/LDH nanocomposite.

the preparation process.[103] The peaks at 1034, 658, and 430 cm^{-1} could be attributed to the M−O and M−O−M stretching vibrations in the LDH.[114] The CuO NPs/Zn−Al LDH nanocomposite showed FTIR peaks that originated from both phases, as shown in Figure 10. Additionally, several peaks shifted to various wavenumbers, such as the peak attributed to the −OH group at 3450 cm^{-1} at 3447 cm^{-1} and the peak attributed to the stretching vibration of OH at 1625 cm^{-1} at 1620 cm^{-1}, demonstrating that LDH and CuO NPs possibly interact via hydrogen bonds.[108,115]

Figure 11a−c show the hydrodynamic particle distributions of the CuO NPs, Zn−Al LDH, and CuO NPs/LDH nanocomposite, respectively. As shown, the formed nanomaterials show large hydrodynamic sizes and broad peaks, indicating aggregation in suspension. The average hydrodynamic sizes of the CuO NPs, Zn−Al LDH, and CuO NPs/LDH nanocomposites were 687, 735, and 528 nm, respectively.

The measurements of the zeta potential provide information on the stability of the synthesized nanomaterials. The surface charge of nanomaterials can indicate how strongly the particles in the suspension repel or are attracted to one another, thereby affecting the stability of the suspension. The zeta potentials of the CuO NPs, Zn−Al LDH, and CuO NPs/LDH nanocomposite are shown in Figure 11d−f and were −21.4, 22.3, and 30.8 mV, respectively. These values indicate that the suspension of such nanomaterials can have a reasonable degree of stability.[1,116] These findings indicate that the high positive zeta potential of the CuO NPs/Zn−Al LDH nanocomposite could be related to the interaction between the biomolecules capping the biosynthesized CuO NPs and the central metal ions in the Zn−Al LDH. The increase in zeta potential after loading CuO NPs onto the LDH was attributed to surface charge modification. Surface charge modification occurs when the CuO NPs have a different charge (−21.3 mV) than the original LDH

https://doi.org/10.1021/acsomega.4c02133
ACS Omega 2024, 9, 34507−34529

Table 5. Zone of Inhibition of CuO NPs, Zn−Al LDH, and CuO NPs/LDH Nanocomposite

concentration (mg/mL)	methicillin-resistant *S. aureus* ATCC 43300	*L. monocytogenes* ATCC 7644	*S. typhimurium* ATCC 14028	*P. aeruginosa* ATCC 9027	*C. albicans* ATCC 60913
CuO NPs inhibition zone (mm)					
0.125	13 ± 0.03	16 ± 0.1	0	15 ± 0.3	16 ± 0.6
0.25	16 ± 0.1	17 ± 0.6	0	18 ± 0.1	19 ± 0.05
0.5	19 ± 0.5	20 ± 0.5	0	22 ± 0.01	21 ± 0.1
1	21 ± 0.13	22 ± 0.04	0	23 ± 0.011	23 ± 0.3
5	22 ± 0.3	25 ± 0.05	23 ± 0.23	26 ± 0.21	24 ± 0.3
Zn−Al LDH inhibition zone (mm)					
0.125	14 ± 0.4	15 ± 0.3	0	15 ± 0.01	13 ± 0.5
0.25	16 ± 0.2	17 ± 0.03	0	17 ± 0.1	15 ± 0.1
0.5	17 ± 0.3	19 ± 0.1	0	20 ± 0.5	18 ± 0.6
1	18 ± 0.6	21 ± 0.04	0	23 ± 0.6	19 ± 0.6
5	25 ± 0.02	22 ± 0.011	21 ± 0.3	24 ± 0.6	22 ± 0.4
CuO NPs/Zn−Al LDH inhibition zone (mm)					
0.125	20 ± 0.03	21 ± 0.4	13 ± 0.06	16 ± 0.5	17 ± 0.25
0.25	23 ± 0.1	23 ± 0.6	15 ± 0.013	19 ± 0.6	19 ± 0.1
0.5	24 ± 0.6	25 ± 0.1	18 ± 0.1	24 ± 0.1	22 ± 0.3
1	26 ± 0.012	26 ± 0.15	20 ± 0.13	26 ± 0.13	24 ± 0.23
5	27 ± 0.18	30 ± 0.34	25 ± 0.17	28 ± 0.03	26 ± 0.21

surface (22.3 mV). A higher charge density of the LDH material can effectively increase the overall zeta potential of the particle. This occurs due to the introduction of more charged species or functional groups and the addition of MO onto the particle surface.[117] A high zeta potential of the material can promote particle stability and prevent aggregation. This ensures a greater surface area and better contact between the material and microorganisms, increasing the chances of antimicrobial interactions and effectiveness.[118,119]

3.6. Antimicrobial Activity Assay. *3.6.1. Zone Detection.* The antimicrobial activity of all the produced materials (CuO NPs, Zn−Al LDH, and CuO NPs/LDH nanocomposite) was evaluated toward yeast (*C. albicans* ATCC 60913), Gram-positive bacteria (*L. monocytogenes* ATCC 7644, methicillin-resistant *S. aureus* ATCC 43300) and Gram-negative bacteria (*S. typhimurium* ATCC 14028, *P. aeruginosa* ATCC 9027) using the agar-well diffusion technique. The inhibition zones of the synthesized nanomaterials at various concentrations (0.125, 0.25, and 0.5 to 1 and 5 mg/mL) showed strong antimicrobial effects on all the tested organisms in a concentration-dependent manner. As shown in Table 5, the inhibition zone increased with increasing concentrations of the synthesized nanomaterials (Figure 12). Furthermore, the results demonstrated that the synthesized nanomaterials were effective against a variety of organisms. DMSO was utilized as a control, while distilled H_2O was used as a blank. DMSO showed no antimicrobial activity against the selected test organisms. On the other hand, CuO NPs showed significant antimicrobial properties against all the tested pathogens, which agrees with the findings of Nabila and Kannabiran, 2018,[100] and Bukhari et al., 2021,[120] who reported that the actinobacteria-mediated synthesis of CuO NPs has an effective antibacterial capability toward both Gram-negative and Gram-positive bacteria. The inhibitory effect of the biosynthesized CuO NPs can be attributed to the high surface area-to-volume ratio of the 3D flower-like structures, which allows better contact with the microbial cell membrane. In addition, this enhanced antibacterial activity can be attributed to the copper ions released from the CuO nanoparticles. These copper ions can penetrate the bacterial cell membrane and disrupt the cell membrane structure by adhering directly to the cell wall, which has a negative charge.[121,122] By binding with microbial DNA molecules, copper ions cause cross-linkage within nucleic acid strands, which can lead to a disordered helical structure of DNA molecules followed by protein denaturation and other cell biochemical processes, ultimately resulting in full destruction of the microbial cell.[123−125] Moreover, Santo et al., 2008[126] revealed the inhibitory effect of CuO NPs associated with a deactivated surface protein responsible for material transport via cytoplasmic membranes and the destruction of selective permeability.

Table 5 shows that the tested pathogens exhibited great sensitivity for the used Zn−Al LDH, which is in agreement with previous research showing that Zn−Al LDH has antimicrobial effects on Gram-positive bacteria, Gram-negative bacteria, and fungi.[127,128] The antimicrobial capability of the prepared Zn−Al LDH may be due to the hydroxyl ions liberated in the aqueous medium. These ions are well-known as extremely oxidizing free radicals that exhibit excessive reactivity with various biomolecules, such as the bacterial cytoplasmic membrane and DNA, and cause the denaturation of proteins.[129] Another explanation for the inhibitory properties of the prepared Zn−Al LDH is that zinc ion release works well not only on bacteria but also on fungi by connecting to microorganism membranes comparable to those of mammalian cells.[130] This zinc ion can penetrate the microbial cell membrane through the membrane pore channel by attaching to the plasma membrane via electrostatic attraction, which decreases cell membrane permeability, leading to the loss of low-molecular-weight metabolites and intracellular ions.[131] Moreover, zinc ions extend both the growth cycle lag phase and the microorganism generation time, which delays the full cell division of each organism.[132] An increase in the concentration of Zn−Al LDH is expected to lead to increase the production of H_2O_2, which in turn will affect the structural integrity of the bacterial cell membrane.[133] This process is likely to result in the release of cellular contents and eventual cell death. Furthermore, the antimicrobial properties of Zn−Al LDH nanoparticles can be attributed to their accumulation on the bacterial surface, where they promote the production of ROS and interact with the bacterial cell wall. These ROS have the ability to cause damage to the bacterial cell wall, as well as important cellular

https://doi.org/10.1021/acsomega.4c02133
ACS Omega 2024, 9, 34507−34529

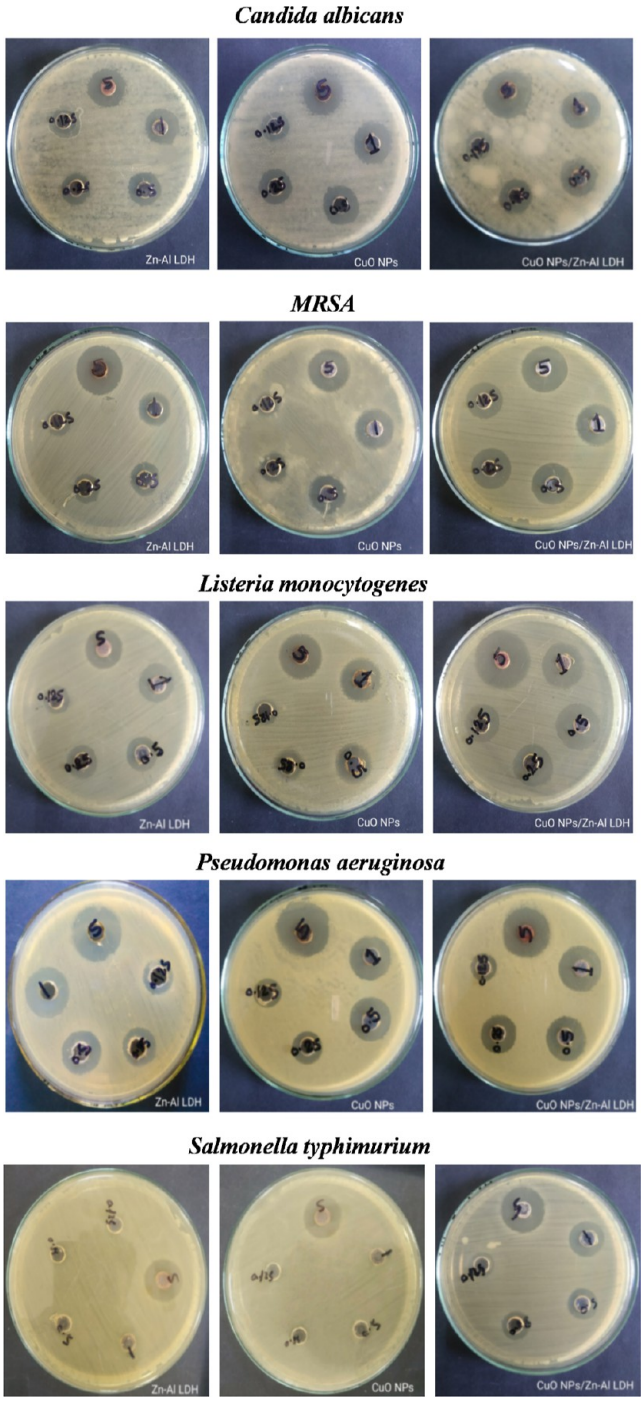

Figure 12. Inhibition zones detected in the well diffusion assay when various pathogens were tested against CuO NPs, Zn−Al LDH, and CuO NPs/Zn−Al LDH nanocomposite.

components such as proteins and nucleic acids, ultimately resulting in the death of the bacterial cells.[133] Figure 13 illustrates the possible antimicrobial mechanisms of the synthesized nanomaterials.

The presence of both phases in the nanocomposite increased the inhibitory efficiency compared to that of either of the single phases, which was revealed by the diameter of the inhibition zones, as shown in Table 5. Other studies in the open literature have shown that a composite can have better antimicrobial activity than its single constituents. For instance, Delgado et al., 2011 illustrated that CuO nanoparticles embedded in polypropylene had better antimicrobial properties than metal copper nanoparticles.[134] Additionally, Syame et al., 2017 reported that the biocidal activity of CuO NPs improved with the addition of chitosan.[135] The superior inhibitory effect of CuO NPs/Zn−Al LDH may be attributed to the inhibitory activity of Cu^{2+} ions from CuO NPs and Zn^{2+} ions from Zn−Al LDH. The release of both ions from the nanocomposite is thought to be the main mechanism behind the observed enhancement in antibacterial activity compared to either phase alone. This is due to the direct interaction between the CuO NPs/Zn−Al LDH nanocomposite and the microbial cell walls, as well as the liberation of antimicrobial ions such as Cu^{2+} and Zn^{2+}. These ions have lethal effects on microbial cells, leading to enhanced antimicrobial efficiency and complete destruction of the cell. The antimicrobial properties of the CuO NPs/Zn−Al LDH nanocomposite can also be attributed to its extremely high surface area, which allows for better interaction with microorganisms. Additionally, the electrostatic attraction between the positively charged surface of the nanocomposite and the negatively charged microbial cell reduces the charge density on the bacterial surface, resulting in a decrease in microbial cell viability. Furthermore, both CuO nanoparticles (NPs) and Zn−Al LDH (LDH) have the ability to produce ROS such as hydroxyl radicals ($OH^{\bullet}$) and superoxide radicals ($O_2^{\bullet-}$). These ROS cause oxidative damage to microorganisms, resulting in the breakdown of cell membranes and subsequent cell death.[136,137] In addition, this composite showed a positive zeta potential (30.8 mV) that was greater than that of the LDH phase (22.3 mV); therefore, the electrostatic attraction toward the bacterial cell wall can be greater. Compared to the nanocomposite, the pure CuO sample showed a zeta potential of −21.4 mV, indicating possible repulsion from the bacterial cell wall. Therefore, Zn−Al LDH support can be thought of not only as an ion release platform for Zn ions but also as a facilitator to facilitate the possible interaction of CuO with the bacterial cell wall. The zeta potential of nanoparticles plays a crucial role in their antimicrobial activity. The results of our experiment showed that the CuO NPs/Zn−Al LDH nanocomposite, with a higher absolute zeta potential (30.8 mV), had a stronger bactericidal effect. This can be attributed to the fact that particles with a greater positive zeta potential are able to form stronger electrostatic interactions with the negatively charged cell membranes of microorganisms. This attractive force allows the nanoparticles to adhere to the microbial surface, potentially leading to increased internalization. Additionally, this enhanced adhesion can disrupt various cellular structures, increase permeability, cause leakage of intracellular components, prevent microbial adhesion and biofilm formation, and ultimately result in cell death. These multifaceted mechanisms collectively contribute to the superior antimicrobial efficacy of nanoparticles with higher positive zeta potentials.[138,139] Several investigations have been conducted to explore the correlation between zeta potential and the effectiveness of antimicrobial substances. In a study conducted by Jastrzębska et al., 2015,[140] it was observed that nanocomposite powders with higher zeta potential values demonstrated commendable antimicrobial properties. Similarly, Oñate-Garzón et al., 2017 also reported an increase in antimicrobial activity when cationic peptides with a greater net charge were utilized.[141] Additionally, Du et al., 2009 presented data indicating that the strength of antibacterial activity was directly associated with the zeta potential of metal-associated CS-NPs.[117] Furthermore, Qi et al., 2004 revealed that the zeta potential of Cu^{2+}-loaded NPs was markedly greater, at

https://doi.org/10.1021/acsomega.4c02133
ACS Omega 2024, 9, 34507−34529

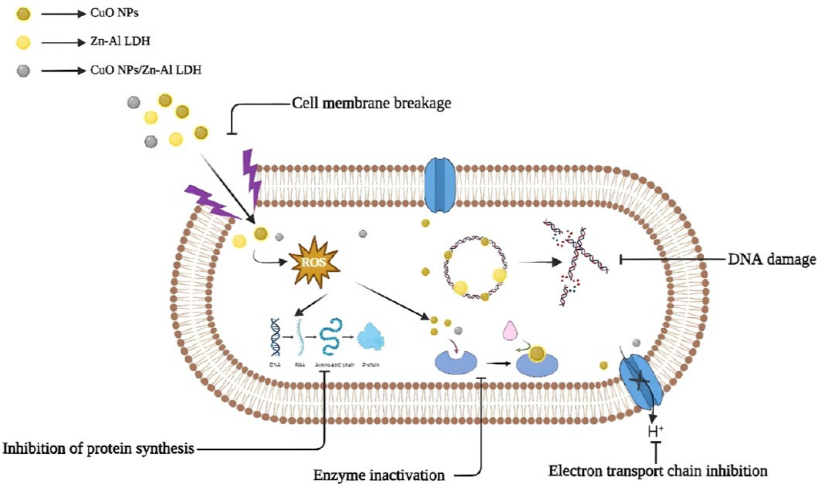

Figure 13. Antimicrobial mechanisms of the synthesized nanomaterials (CuO NPs, Zn−Al LDH, and CuO NPs/Zn−Al LDH nanocomposite).

Table 6. MIC Values for Various Concentrations of the Produced Nanomaterials after 24 h

species	methicillin-resistant *S. aureus* ATCC 43300	*L. monocytogenes* ATCC 7644	*S. typhimurium* ATCC 14028	*P. aeruginosa* ATCC 9027	*C. albicans* ATCC 60913
			CuO NPs		
MIC (μg/mL)	31.25	15.6	—	15.6	62.5
			Zn−Al LDH		
MIC (μg/mL)	62.5	31.25	—	62.5	125
			CuO NPs/Zn−Al LDH		
MIC (μg/mL)	15.6	7.8	125	15.6	31.25

96 mV, than that of CS-NPs, which was recorded at 51 mV. Moreover, Cu^{2+}-loaded CS-NPs displayed greater antibacterial activity than did native CS and slightly surpassed the antibacterial activity of CS-NPs.[142] Numerous research investigations have documented the eco-friendly production of copper oxide nanoparticles (CuO NPs) and zinc−aluminum LDHs (Zn−Al LDH) along with their antibacterial properties, but no previous work has attempted to study the antibacterial properties of such nanocomposites (CuO NPs/Zn−Al LDH). Table 7 presents an overview of the antibacterial properties documented in the literature for biosynthesized CuO NPs and Zn−Al LDH.

3.6.2. MIC Determination. It is important to mention that the MIC values of the synthesized nanomaterials under investigation concerning the previously mentioned bacterial species are shown in Table 6. The MICs of the synthesized nanomaterials differ significantly among species. Furthermore, Table 6 shows that the MICs of the synthesized CuO NPs/Zn−Al LDH nanocomposites decreased compared to those of their individual components. This phenomenon could be attributed to the synergistic antimicrobial impact resulting from the combination of CuO nanoparticles and Zn−Al LDH. This combination enables the effective suppression of bacterial pathogens at much lower concentrations than when the components are used individually.[143]

3.6.3. Time-Kill Curve Assay. The evaluation of time-kill kinetics is crucial for determining the effectiveness and rate of elimination of antimicrobial compounds. Figure 14 shows a significant reduction in the number of colony forming units (cfus) of both *S. aureus* and *C. albicans* after treatment with various substances, including CuO NPs (MIC concentration of 31.25 μg/mL), Zn−Al LDH (MIC concentration of 62.50 μg/mL), CuO NPs/Zn−Al LDH nanocomposite (MIC concentration of 15.6 μg/mL), CuO NPs (MIC concentration of 62.50 μg/mL), Zn−Al LDH (MIC concentration of 125 μg/mL), and CuO NPs/Zn−Al LDH nanocomposite (MIC concentration of 31.25 μg/mL), for both *S. aureus* and *C. albicans*, which resulted in a significant decrease in the cfus of *S. aureus* and *C. albicans*. Interestingly, the most effective eradication of both *S. aureus* and *C. albicans* was observed after 24 h compared to that in the untreated control group.

3.6.4. Assessment of Protein Leakage from the S. aureus Cell Membrane. The quantities of protein released into the suspension from treated *S. aureus* cells were measured using the Bradford method. According to Figure 15, the release of cellular protein from *S. aureus* correlates with the concentration of synthesized CuO NPs, Zn−Al LDH, and CuO NPs/Zn−Al LDH nanocomposites. Specifically, protein concentrations of 86.99, 93.64, and 163.58 μg/mL were detected after treatment with 1.0 mg/mL CuO NPs, Zn−Al LDH and CuO NPs/Zn−Al LDH nanocomposites, respectively. This indicates the antibacterial properties of the nanocomposites, as evidenced by the formation of holes in the cell membrane of *S. aureus*, leading to the leakage of proteins from the cytoplasm. These findings suggest that the CuO NPs/Zn−Al LDH nanocomposite enhances the permeability of the *S. aureus* cell membrane more effectively than do the CuO NPs and Zn−Al LDH, implying that disruption of membrane permeability plays a crucial role in inhibiting bacterial growth. This is supported by similar studies.[144,145] These studies have shown that when Cu ions and Zn ions are introduced, there is a concentration-dependent disruption of bacterial cell membranes, leading to the release of their internal contents into the surrounding medium (bacterial cell suspension).

3.6.5. Ultrastructure of S. aureus Bacteria Treated with CuO NPs, Zn−Al LDH, and CuO NPs/Zn−Al LDH Nano-

https://doi.org/10.1021/acsomega.4c02133
ACS Omega 2024, 9, 34507−34529

Table 7. Overview of the Antibacterial Properties of the Biosynthesized CuO NPs and Zn−Al LDH Reported in the Literature

NPs	microorganisms/synthesized route	shape and size (nm)	antimicrobial activity	refs
CuO	*Streptomyces* MHM38	spherical; 1.72−13.49	against *Enterococcus faecalis* ATCC 29212, *Salmonella typhimurium* ATCC 14028, *Pseudomonas aeruginosa* ATCC 9027, *Escherichia coli* ATCC 8939, *fungi* (*Rhizoctonia solani, Fusarium solani*, and *Aspergillus niger*), and yeast (*Candida albicans* ATCC 10237)	146
	Streptomyces zaomyceticus Oc-5 and *Streptomyces pseudogriseolus* Acv-11	spherical; 78−80	against *Fusarium oxysporum, Pythium ultimum, Aspergillus niger, and Alternaria alternata*	147
	actinomycetes isolate VITBN4	agglomerated clusters; 61.7	against *Staphylococcus aureus, Bacillus cereus, Proteus mirabilis, Edwardsiella tarda, Aeromonas caviae, Aeromonas hydrophila* and *Vibrio anguillarum*	100
	endophytic actinomycetes CKV1	spherical; 20	against *E. coli* and *P. mirabilis*	96
	Streptomyces griseus	spherical; 30−50	against *P. hypolateritia*	111
	Sargassum longifolium	spherical; 40−60	against *Vibrio parahemolyticus, Aeromonas hydrophila, Serratia marcescens and Vibrio harvey*	148
	Bifurcaria bifurcata	spherical; 20.66	against *Escherichia coli and Staphylococcus aureus*	105
	Padina boergesenii	tetragonal crystalline structure; 22−159	against *Bacillus subtilis and Escherichia coli*	149
	Stenotrophomonas sp. BS95	spherical; 35.24 ± 4.64	against *Bacillus subtilis PTCC 1023, Staphylococcus aureus ATCC 25923, Pseudomonas putida KT2440 and Escherichia coli PTCC 1860*	150
	Serratia sp. ZTB29	polydisperse, spherical; 20−40	against *Xanthomonas sp.* and *Alternaria sp*	151
	Brevibacillus brevis PI-5	spherical; 2−28	against *Fusarium oxysporum, Alternaria alternata*, and *Aspergillus niger*	152
	Lactobacillus casei	spherical; 40−110	against *S. aureus*-ATCC-25923 and *P. aeruginosa*-ATCC27853	153
Zn−Al LDH	coprecipitation-hydrothermal method	hexagonal lamellar structure; 176 ± 44	against *Staphylococcus aureus*	69
	coprecipitation	platelets	against *B. subtilis, P. aeruginasa, E. coli* and *S. aureus*	136
	coprecipitation	hexagonal plate-like morphology	against *Escherichia coli* and *Staphylococcus aureus*	154
	separate nucleation and aging steps		against *Staphylococcus aureus* and *Candida albicans*	128
	coprecipitation		against *Escherichia coli and Penicillium cyclopium*	127
CuO NPs/Zn−Al LDH	*Micromonospora* sp. ISP-2 27	hexagonal layered structure and flower-like morphology	against Methicillin-resistant *Staphylococcus aureus* ATCC 43300, *Listeria monocytogenes* ATCC 7644, *Enterococcus faecalis* V583, *E. coli* ATCC 6933, *Pseudomonas aeruginosa* ATCC 9027, and *Candida albicans* ATCC 60913	Present work

https://doi.org/10.1021/acsomega.4c02133
ACS Omega 2024, 9, 34507−34529

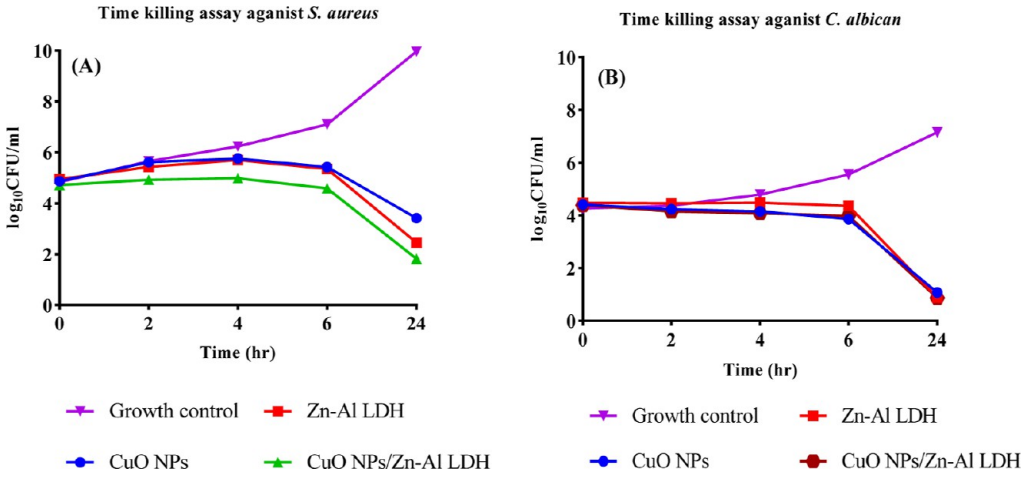

Figure 14. Time-kill curves of the CuO NPs, Zn−Al LDH, and CuO NPs/Zn−Al LDH nanocomposite against (A) *S. aureus* and (B) *C. albicans*.

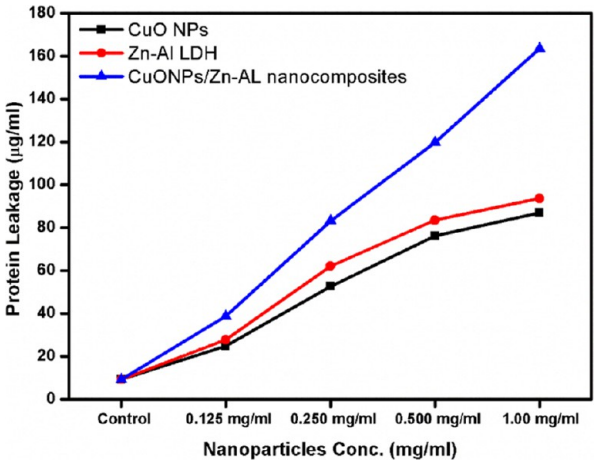

Figure 15. Effect of CuO NPs, Zn−Al LDH, and the CuO NPs/Zn−Al LDH nanocomposite on the protein leakage from *S. aureus* cell membranes.

composite. TEM was utilized to examine the effects of CuO NPs, Zn−Al LDH, and the CuO NPs/Zn−Al LDH nanocomposite on *S. aureus*, specifically observing different types of cellular damage. This study explored the antibacterial action of CuO NPs, Zn−Al LDH, and CuO NPs/Zn−Al LDH nanocomposite by exposing pathogenic microbial cells to 2xMIC in a PDA liquid media for a period of 24 h. As shown in Figure 16a, the TEM observations indicated that the control group cells did not exhibit significant damage, including the absence of pit formation or cell wall rupture. The cell wall appears to be well-defined, and the internal contents of the cells are homogeneously distributed. The cells maintain their characteristic spherical shape. Figure 16b shows that CuO NPs appear to have some irregularities in the cell walls of *S. aureus* cells, with slight indentations that could indicate the beginning stages of CuO NPs interaction. The internal structure of the cells shows some heterogeneity, which might be a sign of stress or damage. However, the overall morphology of the bacteria remains relatively intact, and there is no clear evidence of extensive damage or leakage of cellular contents. Zn−Al LDH had a more pronounced effect on the cells (Figure 16c). The cell walls are visibly compromised, with significant indentations and disruptions. The internal contents of the cells appear to leak out, which is a strong indicator of the cytotoxic effects of nanoparticles. Compared with those of CuO NPs, the morphology of the cells was altered, and the damage was more severe, suggesting a greater degree of Zn-AL LDH interaction and effect. Figure 16d shows the most severe effects of the CuO NPs/Zn−Al nanocomposite interaction on bacterial cells. The bacterial cells are heavily damaged, with large portions of the cell walls disintegrated or completely missing. The internal contents of the cells are extensively leaked into the surrounding area, indicating a high degree of cytotoxicity. The cells lost their characteristic shape and were no longer intact, which is consistent with the strong antibacterial effect of the nanocomposite. The results from the TEM images suggest that the nanocomposite can have a significant impact on the viability and integrity of *S. aureus* cells. The observed damage to the cell walls and the leakage of cellular contents are indicative of the ability of the nanoparticles to disrupt bacterial membranes, which is a common mechanism of antibacterial action. This disruption can lead to cell death and is a promising avenue for the development of new antibacterial treatments, especially in the face of increasing antibiotic resistance.

This combination of CuO and Zn−Al LDH can be further investigated in numerous applications. In addition, other oxides or a mixture of different oxides can be used instead of CuO. Similarly, LDH phases with different chemical properties can be used instead of Zn−Al LDH. These combinations can be investigated for their antibacterial, antiviral, and antifungal properties. Promising candidates can be investigated for applications such as antibacterial clothing, face masks, protective clothing, and antibacterial sprays.

4. CONCLUSIONS

In the present work, a combined MO/LDH nanocomposite was investigated to study its possible enhancement in antimicrobial properties compared to those of the individual phases. No such combination has been reported before in the open literature. A facile method to produce CuO NPs/Zn−Al LDH nanocomposite using a two-stage technique was followed. In the first stage, Zn−Al LDH was synthesized using a simple coprecipitation process. The second stage involves reducing Cu metal ions utilizing cell-free supernatant from *Micromonospora* sp. ISP-2 27, which is subsequently oxidized to form CuO flower-like structures on the surface of Zn−Al LDH. The prepared nanocomposite was characterized using XRD, FTIR, SEM, EDX, zeta potential, and hydrodynamic particle size

https://doi.org/10.1021/acsomega.4c02133
ACS Omega 2024, 9, 34507−34529

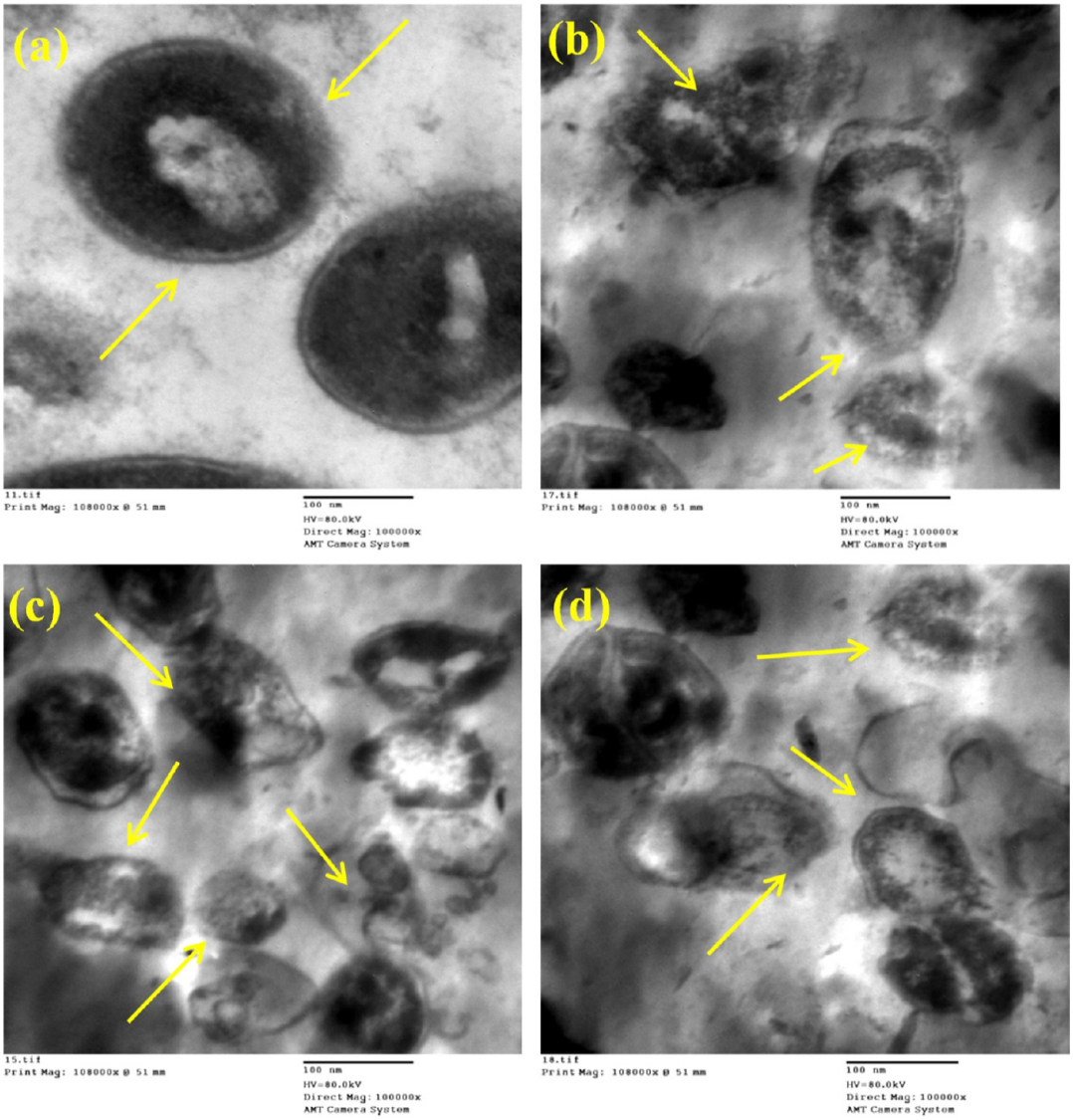

Figure 16. TEM images of *S. aureus* treated with synthesized materials, (a) healthy *S. aureus* cells, (b) *S. aureus* treated with CuO NPs, (c) *S. aureus* treated with Zn−Al LDH, and (d) *S. aureus* treated with CuO NPs/Zn−Al LDH nanocomposite.

analyses. The characterization techniques showed the successful incorporation of CuO flower-like particles on the surface of the LDH phase, which showed a typical hexagonal layered structure. The formed CuO phase was coated with biomolecules originating from the cell-free supernatant used during the preparation procedure, as revealed by the FTIR spectra. The antimicrobial activity of the produced CuO NPs/Zn−Al LDH nanocomposite, as well as the individual CuO NPs and Zn−Al LDH, was tested against Gram-negative bacteria (*S. typhimurium* ATCC 14028, *P. aeruginosa* ATCC 9027), Gram-positive bacteria (methicillin-resistant *S. aureus* ATCC 43300, *L. monocytogenes* ATCC 7644), and yeast (*C. albicans* ATCC 60913). The results showed that the zones of inhibition for the CuO NPs/Zn−Al LDH nanocomposite were greater than those for CuO NPs or Zn−Al LDH alone. This shows that the synergy between the MO and the LDH phase can enhance the performance of the nanocomposite compared to that of either individual phase. This work paves the way toward investigating more MO/LDH composites with different chemistries and morphologies that may prove to possess significant antimicrobial properties and could be promising candidates for several biomedical and bioengineering applications. Such composites are expected to decrease the cost of implementation of such applications due to their low cost of preparation and ease of synthesis. In addition, such composites are expected to show promising results compared to currently reported materials due to their versatile chemistries, morphologies, sizes, and synergistic effects of combining MO and LDH phases. Our future goal is to design a wider range of nanocomposites with enhanced properties. For instance, instead of solely utilizing binary LDH, we aim to incorporate ternary LDH. Additionally, we plan to move away from using monometallic nanoparticles and instead incorporate bimetallic and trimetallic nanoparticles to further enhance the properties of our nanocomposites.

■ ASSOCIATED CONTENT

Data Availability Statement

The data sets used and/or analyzed during the current study are available from the corresponding author upon reasonable request.

https://doi.org/10.1021/acsomega.4c02133
ACS Omega 2024, 9, 34507−34529

AUTHOR INFORMATION

Corresponding Author

Rehab Mahmoud − *Department of Chemistry, Faculty of Science, Beni-Suef University, Beni-Suef 62511, Egypt;* orcid.org/0000-0003-2274-2016; Email: rehabkhaled@science.bsu.edu.eg

Authors

Abdullah A. Eweis − *Department of Botany and Microbiology, Faculty of Science, Beni-Suef University, Beni-Suef 62511, Egypt*

Maged S. Ahmad − *Department of Botany and Microbiology, Faculty of Science, Beni-Suef University, Beni-Suef 62511, Egypt*

Ehab B. El Domany − *Biotechnology and Life Sciences Department, Faculty of Postgraduate Studies for Advanced Sciences, Beni-Suef University, Beni-Suef 62511, Egypt*

Mohammed Al-Zharani − *Department of Biology, College of Science, Imam Mohammad Ibn Saud Islamic University, Riyadh 11623, Saudi Arabia*

Mohammed Mubarak − *Department of Biology, College of Science, Imam Mohammad Ibn Saud Islamic University, Riyadh 11623, Saudi Arabia;* orcid.org/0000-0002-7160-8297

Zienab E Eldin − *Department of Materials Science and Nanotechnology, Faculty of Postgraduate Studies for Advanced Sciences, Beni-Suef University, Beni-Suef 62511, Egypt*

Yasser GadelHak − *Department of Materials Science and Nanotechnology, Faculty of Postgraduate Studies for Advanced Sciences, Beni-Suef University, Beni-Suef 62511, Egypt;* orcid.org/0000-0001-5186-160X

Wael N. Hozzein − *Department of Botany and Microbiology, Faculty of Science, Beni-Suef University, Beni-Suef 62511, Egypt;* orcid.org/0000-0003-2467-9719

Complete contact information is available at: https://pubs.acs.org/10.1021/acsomega.4c02133

Author Contributions

Abdullah A. Eweis, Maged S. Ahmad, and Ehab B. El Domany were responsible for the antibacterial study. Abdullah A. Eweis, Yasser GadelHak, and Rehab Mahmoud were responsible for the nanomaterial synthesis and characterization study. Mohammed Al-Zharani, Mohammed Mubarak, Wael N. Hozzein and Rehab Mahmoud were responsible for funding, management, and supervision.

Funding

This work was supported and funded by the Deanship of Scientific Research at Imam Mohammad Ibn Saud Islamic University (IMSIU) (grant number IMSIU-RP23091).

Notes

The authors declare no competing financial interest.

ACKNOWLEDGMENTS

We would like to express our gratitude to all those who have contributed to the completion of this research. We thank the Deanship of Scientific Research at Imam Mohammad Ibn Saud Islamic University for their financial support under grant number IMSIU-RP23091. We are also grateful to Botany and Microbiology Department for providing the necessary facilities and resources. Special thanks to M.S.A., W.H.N., and R.M. for their invaluable assistance and insightful discussions during the research process. We also appreciate the support and encouragement from our family and friends.

REFERENCES

(1) Składanowski, M.; Wypij, M.; Laskowski, D.; Golińska, P.; Dahm, H.; Rai, M. Silver and gold nanoparticles synthesized from Streptomyces sp. isolated from acid forest soil with special reference to its antibacterial activity against pathogens. *J. Cluster Sci.* **2017**, *28* (1), 59−79.

(2) Mancuso, G.; Midiri, A.; Gerace, E.; Biondo, C. Bacterial antibiotic resistance: The most critical pathogens. *Pathogens* **2021**, *10* (10), 1310.

(3) Datta, P.; Gupta, V. Next-generation strategy for treating drug resistant bacteria: Antibiotic hybrids. *Indian J. Med. Res.* **2019**, *149* (2), 97.

(4) Mubeen, B.; Ansar, A. N.; Rasool, R.; Ullah, I.; Imam, S. S.; Alshehri, S.; Ghoneim, M. M.; Alzarea, S. I.; Nadeem, M. S.; Kazmi, I. Nanotechnology as a novel approach in combating microbes providing an alternative to antibiotics. *Antibiotics* **2021**, *10* (12), 1473.

(5) Xie, M.; Gao, M.; Yun, Y.; Malmsten, M.; Rotello, V. M.; Zboril, R.; Akhavan, O.; Kraskouski, A.; Amalraj, J.; Cai, X.; et al. Antibacterial nanomaterials: mechanisms, impacts on antimicrobial resistance and design principles. *Angew. Chem., Int. Ed.* **2023**, *62* (17), No. e202217345.

(6) Wang, Y.; Yang, Y.; Shi, Y.; Song, H.; Yu, C. Antibiotic-free antibacterial strategies enabled by nanomaterials: progress and perspectives. *Adv. Mater.* **2020**, *32* (18), 1904106.

(7) León-Buitimea, A.; Garza-Cervantes, J. A.; Gallegos-Alvarado, D. Y.; Osorio-Concepción, M.; Morones-Ramírez, J. R. Nanomaterial-based antifungal therapies to combat fungal diseases aspergillosis, Coccidioidomycosis, Mucormycosis, and candidiasis. *Pathogens* **2021**, *10* (10), 1303.

(8) Sousa, F.; Ferreira, D.; Reis, S.; Costa, P. Current insights on antifungal therapy: Novel nanotechnology approaches for drug delivery systems and new drugs from natural sources. *Pharmaceuticals* **2020**, *13* (9), 248.

(9) Chakravarty, M.; Vora, A. Nanotechnology-based antiviral therapeutics. *Drug Delivery Transl. Res.* **2021**, *11*, 748−787.

(10) Zhou, J.; Krishnan, N.; Jiang, Y.; Fang, R. H.; Zhang, L. Nanotechnology for virus treatment. *Nano Today* **2021**, *36*, 101031.

(11) Şen Karaman, D.; Ercan, U. K.; Bakay, E.; Topaloğlu, N.; Rosenholm, J. M. Evolving technologies and strategies for combating antibacterial resistance in the advent of the postantibiotic era. *Adv. Funct. Mater.* **2020**, *30* (15), 1908783.

(12) Muteeb, G. Nanotechnology—A Light of Hope for Combating Antibiotic Resistance. *Microorganisms* **2023**, *11* (6), 1489.

(13) Jose, J. K.; Cherian, C. T.; Balachandran, M. A Review on Advanced Nanomaterials for Antibacterial Applications. *Curr. Nanosci.* **2023**, *19* (6), 803−816.

(14) Oves, M.; Rauf, M. A.; Ansari, M. O.; Aslam Parwaz Khan, A.; A Qari, H.; Alajmi, M. F.; Sau, S.; Iyer, A. K. Graphene Decorated Zinc Oxide and Curcumin to Disinfect the Methicillin-Resistant Staphylococcus aureus. *Nanomaterials* **2020**, *10* (5), 1004.

(15) Oves, M.; Aslam, M.; Rauf, M. A.; Qayyum, S.; Qari, H. A.; Khan, M. S.; Alam, M. Z.; Tabrez, S.; Pugazhendhi, A.; Ismail, I. M. Antimicrobial and anticancer activities of silver nanoparticles synthesized from the root hair extract of Phoenix dactylifera. *Mater. Sci. Eng., C* **2018**, *89*, 429−443.

(16) Tsikourkitoudi, V.; Henriques-Normark, B.; Sotiriou, G. A. Inorganic nanoparticle engineering against bacterial infections. *Curr. Opin. Chem. Eng.* **2022**, *38*, 100872.

(17) Karnwal, A.; Kumar, G.; Pant, G.; Hossain, K.; Ahmad, A.; Alshammari, M. B. Perspectives on Usage of Functional Nanomaterials in Antimicrobial Therapy for Antibiotic-Resistant Bacterial Infections. *ACS Omega* **2023**, *8* (15), 13492−13508.

(18) Jawad Ahmad, F. Nanoparticles in the Era of Antimicrobial Resistance. *Pakistan BioMed. J.* **2022**, *5*, 01.

(19) Natan, M.; Banin, E. From Nano to Micro: using nanotechnology to combat microorganisms and their multidrug resistance. *FEMS Microbiol. Rev.* **2017**, *41* (3), 302−322.

(20) Hetta, H. F.; Ramadan, Y. N.; Al-Harbi, A. I. A.; A Ahmed, E.; Battah, B.; Abd Ellah, N. H.; Zanetti, S.; Donadu, M. G. Nanotechnology as a Promising Approach to Combat Multidrug Resistant Bacteria: A Comprehensive Review and Future Perspectives. *Biomedicines* **2023**, *11* (2), 413.
(21) Hochvaldová, L.; Večeřová, R.; Kolář, M.; Prucek, R.; Kvítek, L.; Lapčík, L.; Panáček, A. Antibacterial nanomaterials: Upcoming hope to overcome antibiotic resistance crisis. *Nanotechnol. Rev.* **2022**, *11* (1), 1115−1142.
(22) Gu, X.; Xu, Z.; Gu, L.; Xu, H.; Han, F.; Chen, B.; Pan, X. Preparation and antibacterial properties of gold nanoparticles: A review. *Environ. Chem. Lett.* **2021**, *19*, 167−187.
(23) Jeyasundari, J.; Praba, P. S.; Jacob, Y. B. A.; Vasantha, V.; Shanmugaiah, V. Green synthesis and characterization of zero valent iron nanoparticles from the leaf extract of Psidium guajava plant and their antibacterial activity. *Chem. Sci. Rev. Lett.* **2017**, *6* (22), 1244−1252.
(24) Sedaghat Anbouhi, T.; Esfidvajani, E. M.; Nemati, F.; Haghighat, S.; Sari, S.; Attar, F.; Pakaghideh, A.; Sohrabi, M. J.; Mousavi, S. E.; Falahati, M. Albumin binding, anticancer and antibacterial properties of synthesized zero valent iron nanoparticles. *Int. J. Nanomed.* **2019**, *14*, 243−256.
(25) Amin, R. M.; Mahmoud, R. K.; Gadelhak, Y.; Abo El-Ela, F. I. Gamma irradiated green synthesized zero valent iron nanoparticles as promising antibacterial agents and heavy metal nano-adsorbents. *Environ. Nanotechnol., Monit. Manage.* **2021**, *16*, 100461.
(26) Din, M. I.; Arshad, F.; Hussain, Z.; Mukhtar, M. Green adeptness in the synthesis and stabilization of copper nanoparticles: catalytic, antibacterial, cytotoxicity, and antioxidant activities. *Nanoscale Res. Lett.* **2017**, *12*, 638.
(27) Rajeshkumar, S.; Menon, S.; Venkat Kumar, S.; Tambuwala, M. M.; Bakshi, H. A.; Mehta, M.; Satija, S.; Gupta, G.; Chellappan, D. K.; Thangavelu, L.; et al. Antibacterial and antioxidant potential of biosynthesized copper nanoparticles mediated through Cissus arnotiana plant extract. *J. Photochem. Photobiol., B* **2019**, *197*, 111531.
(28) Guimier, E.; Carson, L.; David, B.; Lambert, J. M.; Zupansic, J.; Heery, E.; Malcolm, R. K. Incorporation of copper and zinc nanoparticles and salts into medical-grade silicone as antibacterial candidates for prevention of capsular contracture. In *Controlled Release Society 2023 Annual Meeting*, 2023.
(29) Jayandran, M.; Haneefa, M. M.; Balasubramanian, V. Synthesis, Characterization and antimicrobial activities of turmeric curcumin and curcumin stabilized zinc nanoparticles-A green approach. *Res. J. Pharm. Technol.* **2015**, *8* (4), 445−451.
(30) Hassan, S. S.; Al-Haddad, R. M.; Hubeatir, K. A. Temperature effects on the optical properties of bismuth nanoparticles prepared by PLAL for antibacterial activity. *Int. J. Nanoelectron. Mater.* **2023**, *16*, 81.
(31) Rieznichenko, L. S.; Gruzina, T.; Dybkova, S.; Ushkalov, V.; Ulberg, Z. Investigation of bismuth nanoparticles antimicrobial activity against high pathogen microorganisms. *Am. J. Bioterror. Biosecur. Biodef.* **2015**, *2*, 1004.
(32) Majeed, H. M.; Wadee, S. A. Antibacterial activity and mechanism of nickel nanoparticles against multidrug resistant pseudomonas aeruginosa. *Ann. Trop. Med. Public Health* **2019**, *22*, 157−168.
(33) Mohindru, J. J.; Garg, U. Sol-gel synthesis of copper, silver, and nickel nanoparticles and comparison of their antibacterial activity. *Int. J. Theor. Appl. Sci.* **2017**, *9*, 151−156.
(34) P, A. J.; M, S.; J, D. R.; S, S. S. Pyrimidine Derivative Schiff Base Ligand Stabilized Copper and Nickel Nanoparticles by Two Step Phase Transfer Method; in Vitro Anticancer, Antioxidant, Anti-Microbial and DNA Interactions. *J. Fluoresc.* **2020**, *30* (3), 471−482.
(35) Hameed, W. F.; Owaid, Y. H.; Noomi, B. S.; Nada, A. H. Silver and Cobalt nanoparticles as potential antibacterial agents Staphylococcus aureus isolated from wound infections. *J. Pure Sci.* **2020**, *25* (2), 21.
(36) Helen, S. M.; Rani, S. H. Characterization and Antimicrobial Study of Cobalt Nanoparticles Synthesized from Manihot Esculent (Tapioca) by Green Route. *Int. J. Sci. Res. Dev.* **2015**, *3*, 440.
(37) Slavin, Y. N.; Asnis, J.; Hńfeli, U. O.; Bach, H. Metal nanoparticles: understanding the mechanisms behind antibacterial activity. *J. Nanobiotechnol.* **2017**, *15*, 65.
(38) Naseem, T.; Durrani, T. The role of some important metal oxide nanoparticles for wastewater and antibacterial applications: A review. *Environ. Chem. Ecotoxicol.* **2021**, *3*, 59−75.
(39) Sirelkhatim, A.; Mahmud, S.; Seeni, A.; Kaus, N. H. M.; Ann, L. C.; Bakhori, S. K. M.; Hasan, H.; Mohamad, D. Review on zinc oxide nanoparticles: antibacterial activity and toxicity mechanism. *Nano-Micro Lett.* **2015**, *7*, 219−242.
(40) Lallo da Silva, B.; Abuçafy, M. P.; Berbel Manaia, E.; Oshiro Junior, J. A.; Chiari-Andréo, B. G.; Pietro, R. C. R.; Chiavacci, L. A. Relationship between structure and antimicrobial activity of zinc oxide nanoparticles: An overview. *Int. J. Nanomed.* **2019**, *14*, 9395−9410.
(41) Sabouri, Z.; Akbari, A.; Hosseini, H. A.; Khatami, M.; Darroudi, M. Green-based bio-synthesis of nickel oxide nanoparticles in Arabic gum and examination of their cytotoxicity, photocatalytic and antibacterial effects. *Green Chem. Lett. Rev.* **2021**, *14* (2), 404−414.
(42) Moghadam, N. C. Z.; Jasim, S. A.; Ameen, F.; Alotaibi, D. H.; Nobre, M. A.; Sellami, H.; Khatami, M. RETRACTED ARTICLE: Nickel oxide nanoparticles synthesis using plant extract and evaluation of their antibacterial effects on Streptococcus mutans. *Bioprocess Biosyst. Eng.* **2022**, *45* (7), 1201−1210.
(43) Ezealigo, U. S.; Ezealigo, B. N.; Aisida, S. O.; Ezema, F. I. Iron oxide nanoparticles in biological systems: Antibacterial and toxicology perspective. *JCIS Open* **2021**, *4*, 100027.
(44) Ismail, R. A.; Sulaiman, G. M.; Abdulrahman, S. A.; Marzoog, T. R. Antibacterial activity of magnetic iron oxide nanoparticles synthesized by laser ablation in liquid. *Mater. Sci. Eng., C* **2015**, *53*, 286−297.
(45) Gudkov, S. V.; Burmistrov, D. E.; Serov, D. A.; Rebezov, M. B.; Semenova, A. A.; Lisitsyn, A. B. Do iron oxide nanoparticles have significant antibacterial properties? *Antibiotics* **2021**, *10* (7), 884.
(46) Khan, S.; Ansari, A. A.; Khan, A. A.; Ahmad, R.; Al-Obaid, O.; Al-Kattan, W. In vitro evaluation of anticancer and antibacterial activities of cobalt oxide nanoparticles. *JBIC, J. Biol. Inorg. Chem.* **2015**, *20*, 1319−1326.
(47) Moradpoor, H.; Safaei, M.; Rezaei, F.; Golshah, A.; Jamshidy, L.; Hatam, R.; Abdullah, R. S. Optimisation of cobalt oxide nanoparticles synthesis as bactericidal agents. *Open Access Maced. J. Med. Sci.* **2019**, *7* (17), 2757−2762.
(48) Chelliah, P.; Wabaidur, S. M.; Sharma, H. P.; Jweeg, M. J.; Majdi, H. S. A. L.; AL Kubaisy, M. M. R.; Iqbal, A.; Lai, W.-C. Green synthesis and characterizations of cobalt oxide nanoparticles and their coherent photocatalytic and antibacterial investigations. *Water* **2023**, *15* (5), 910.
(49) Gudkov, S. V.; Burmistrov, D. E.; Smirnova, V. V.; Semenova, A. A.; Lisitsyn, A. B. A mini review of antibacterial properties of Al2O3 nanoparticles. *Nanomaterials* **2022**, *12* (15), 2635.
(50) Szunerits, S.; Boukherroub, R. Antibacterial activity of graphene-based materials. *J. Mater. Chem. B* **2016**, *4* (43), 6892−6912.
(51) Shi, L.; Chen, J.; Teng, L.; Wang, L.; Zhu, G.; Liu, S.; Luo, Z.; Shi, X.; Wang, Y.; Ren, L. The antibacterial applications of graphene and its derivatives. *Small* **2016**, *12* (31), 4165−4184.
(52) He, J.; Zhu, X.; Qi, Z.; Wang, C.; Mao, X.; Zhu, C.; He, Z.; Li, M.; Tang, Z. Killing dental pathogens using antibacterial graphene oxide. *ACS Appl. Mater. Interfaces* **2015**, *7* (9), 5605−5611.
(53) Barbolina, I.; Woods, C.; Lozano, N.; Kostarelos, K.; Novoselov, K.; Roberts, I. Purity of graphene oxide determines its antibacterial activity. *2D Materials* **2016**, *3* (2), 025025.
(54) Nanda, S. S.; Yi, D. K.; Kim, K. Study of antibacterial mechanism of graphene oxide using Raman spectroscopy. *Sci. Rep.* **2016**, *6* (1), 28443.
(55) Mocan, T.; Matea, C. T.; Pop, T.; Mosteanu, O.; Buzoianu, A. D.; Suciu, S.; Puia, C.; Zdrehus, C.; Iancu, C.; Mocan, L. Carbon nanotubes as anti-bacterial agents. *Cell. Mol. Life Sci.* **2017**, *74*, 3467−3479.
(56) Mohammed, M. K.; Mohammad, M.; Jabir, M. S.; Ahmed, D. Functionalization, characterization, and antibacterial activity of single wall and multi wall carbon nanotubes. In *IOP Conference Series: Materials Science and Engineering*; IOP Publishing, 2020; p 012028.

https://doi.org/10.1021/acsomega.4c02133
ACS Omega 2024, 9, 34507−34529

(57) Gu, Z.; Atherton, J. J.; Xu, Z. P. Hierarchical layered double hydroxide nanocomposites: structure, synthesis and applications. *Chem. Commun.* **2015**, *51* (15), 3024−3036.
(58) Mahmoud, R.; Safwat, N.; Fathy, M.; Mohamed, N. A.; El-Dek, S.; El-Banna, H. A.; Farghali, A.; Abo El-Ela, F. I. Novel anti-inflammatory and wound healing controlled released LDH-Curcumin nanocomposite via intramuscular implantation, in-vivo study. *Arabian J. Chem.* **2022**, *15* (3), 103646.
(59) Yang, Q.-Z.; Chang, Y.-Y.; Zhao, H.-Z. Preparation and antibacterial activity of lysozyme and layered double hydroxide nanocomposites. *Water Res.* **2013**, *47* (17), 6712−6718.
(60) Kiani, M.; Bagherzadeh, M.; Ghadiri, A. M.; Makvandi, P.; Rabiee, N. Multifunctional green synthesized Cu-Al layered double hydroxide (LDH) nanoparticles: anti-cancer and antibacterial activities. *Sci. Rep.* **2022**, *12* (1), 9461.
(61) Awassa, J.; Cornu, D.; Soulé, S.; Carteret, C.; Ruby, C.; El-Kirat-Chatel, S. Divalent metal release and antimicrobial effects of layered double hydroxides. *Appl. Clay Sci.* **2022**, *216*, 106369.
(62) Cardinale, A. M.; Vecchio Ciprioti, S.; Fortunato, M.; Catauro, M. Thermal behavior and antibacterial studies of a carbonate Mg-Al-based layered double hydroxide (LDH) for in vivo uses. *J. Therm. Anal. Calorim.* **2023**, *148* (4), 1523−1532.
(63) Wang, Q.; Liao, C.; Liu, B.; Jing, S.; Guo, Z.; Liang, L.; Liu, J.; Li, N.; Zhou, R.; Baker, I.; et al. Enhanced corrosion resistance, antibacterial properties and osteogenesis by Cu ion optimized MgAl-layered double hydroxide on Mg alloy. *J. Magnesium Alloys* **2023**.
(64) Abdel Aziz, S. A. A.; GadelHak, Y.; Mohamed, M. B. E. D.; Mahmoud, R. Antimicrobial properties of promising Zn-Fe based layered double hydroxides for the disinfection of real dairy wastewater effluents. *Sci. Rep.* **2023**, *13* (1), 7601.
(65) Elkartehi, M. E.; Zaher, A.; Farghali, A.; Ma, M.; Mahmoud, R.; Shehata, N. Antibacterial activities of layer double hydroxide nanocubes based on Zeolite templates and its high performance as a disinfectant. *Egypt. J. Chem.* **2023**, *66* (3), 265−270.
(66) Mohamed, H.; Mahmoud, R.; Abdelwahab, A.; Farghali, A. A.; Abo El-Ela, F. I.; Allah, A. E. Multifunctional ternary ZnMgFe LDH as an efficient adsorbent for ceftriaxone sodium and antimicrobial agent: sustainability of adsorption waste as a catalyst for methanol electro-oxidation. *RSC Adv.* **2023**, *13* (37), 26069−26088.
(67) Sayed, H.; Mahmoud, R.; Mohamed, H. F.; Gaber, Y.; Shehata, N. Co and Ni double substituted Zn-Fe layered double hydroxide as 2d nano-adsorbent for wastewater treatment. *Key Eng. Mater.* **2022**, *922*, 193−213.
(68) Mishra, G.; Dash, B.; Pandey, S.; Sethi, D. Ternary layered double hydroxides (LDH) based on Cu-substituted ZnAl for the design of efficient antibacterial ceramics. *Appl. Clay Sci.* **2018**, *165*, 214−222.
(69) Awassa, J.; Soulé, S.; Cornu, D.; Ruby, C.; El-Kirat-Chatel, S. Understanding the role of surface interactions in the antibacterial activity of layered double hydroxide nanoparticles by atomic force microscopy. *Nanoscale* **2022**, *14* (29), 10335−10348.
(70) Nguyen, V. T.; Vu, V. T.; Nguyen, T. H.; Nguyen, T. A.; Tran, V. K.; Nguyen-Tri, P. Antibacterial activity of TiO2-and ZnO-decorated with silver nanoparticles. *J. Compos. Sci.* **2019**, *3* (2), 61.
(71) Asamoah, R.; Annan, E.; Mensah, B.; Nbelayim, P.; Apalangya, V.; Onwona-Agyeman, B.; Yaya, A. A comparative study of antibacterial activity of CuO/Ag and ZnO/Ag nanocomposites. *J. Compos. Sci.* **2020**, *2020*, 1−18.
(72) Pavithra, M.; Jessie Raj, M. Synthesis of ultrasonic assisted co-precipitated Ag/ZnO nanorods and their profound anti-liver cancer and antibacterial properties. *Mater. Sci. Eng., B* **2022**, *278*, 115653.
(73) Cao, D.; Xu, Z.; Chen, Y.; Ke, Q.; Zhang, C.; Guo, Y. Ag-loaded MgSrFe-layered double hydroxide/chitosan composite scaffold with enhanced osteogenic and antibacterial property for bone engineering tissue. *J. Biomed. Mater. Res., Part B* **2018**, *106* (2), 863−873.
(74) Marcato, P. D.; Parizotto, N. V.; Martinez, D. S. T.; Paula, A. J.; Ferreira, I. R.; Melo, P. S.; Durán, N.; Alves, O. L. New hybrid material based on layered double hydroxides and biogenic silver nanoparticles: antimicrobial activity and cytotoxic effect. *J. Braz. Chem. Soc.* **2013**, *24*, 266−272.
(75) Carja, G.; Kameshima, Y.; Nakajima, A.; Dranca, C.; Okada, K. Nanosized silver-anionic clay matrix as nanostructured ensembles with antimicrobial activity. *Int. J. Antimicrob. Agents* **2009**, *34* (6), 534−539.
(76) Engin, A. B. Combined Toxicity of Metal Nanoparticles: Comparison of Individual and Mixture Particles Effect. In *Protein Kinase-mediated Decisions Between Life and Death*; Engin, A. B., Engin, A., Eds.; Springer International Publishing: Cham, 2021; pp 165−193.
(77) Mu, Y.; Jia, F.; Ai, Z.; Zhang, L. Iron oxide shell mediated environmental remediation properties of nano zero-valent iron. *Environ. Sci.: Nano* **2017**, *4* (1), 27−45.
(78) Madan, S.; Shaw, R.; Tiwari, S.; Tiwari, S. K. Enhancing corrosion stability and shelf life of nanoscale zero-valent iron via encapsulation in porous Ze-TiO2 matrix: An interface for simultaneous oxidation and adsorption of As (III). *Colloids Surf., A* **2020**, *607*, 125381.
(79) Rasouli, N.; Movahedi, M.; Doudi, M. Synthesis and characterization of inorganic mixed metal oxide nanoparticles derived from Zn-Al layered double hydroxide and their antibacterial activity. *Surf. Interfaces* **2017**, *6*, 110−115.
(80) Okami, Y.; Suzuki, M. A simple method for microscopical observation of Streptomycetes and critique of Streptomyces grouping with reference to aerial structure. *J. Antibiot., Ser. A* **1958**, *11* (6), 250−253.
(81) Pridham, T. G.; Anderson, P.; Foley, C.; Lindenfelser, L.; Hesseltine, C.; Benedict, R. A selection of media for maintenance and taxonomic study of streptomycetes. *Antibiot. Annu.* **1957**, 947−953.
(82) Shirling, E. B.; Gottlieb, D. Methods for characterization of Streptomyces species. *Int. J. Syst. Bacteriol.* **1966**, *16* (3), 313−340.
(83) Pridham, T.; Gottlieb, D. The utilization of carbon compounds by some Actinomycetales as an aid for species determination. *J. Bacteriol.* **1948**, *56* (1), 107−114.
(84) Risdian, C.; Landwehr, W.; Rohde, M.; Schumann, P.; Hahnke, R. L.; Spröer, C.; Bunk, B.; Kämpfer, P.; Schupp, P. J.; Wink, J. Streptomyces bathyalis sp. nov., an actinobacterium isolated from the sponge in a deep sea. *Antonie van Leeuwenhoek* **2021**, *114*, 425−435.
(85) Jones, K. L. Fresh isolates of actinomycetes in which the presence of sporogenous aerial mycelia is a fluctuating characteristic. *J. Bacteriol.* **1949**, *57* (2), 141−145.
(86) Sierra, G. A simple method for the detection of lipolytic activity of micro-organisms and some observations on the influence of the contact between cells and fatty substrates. *Antonie van Leeuwenhoek* **1957**, *23*, 15−22.
(87) Kim, B.; Al-Tai, A. M.; Kim, S. B.; Somasundaram, P.; Goodfellow, M. Streptomyces thermocoprophilus sp. nov., a cellulase-free endo-xylanase-producing streptomycete. *Int. J. Syst. Evol. Microbiol.* **2000**, *50* (2), 505−509.
(88) Chun, J.; Goodfellow, M. A phylogenetic analysis of the genus Nocardia with 16S rRNA gene sequences. *Int. J. Syst. Evol. Microbiol.* **1995**, *45* (2), 240−245.
(89) Thompson, J. D.; Higgins, D. G.; Gibson, T. J. CLUSTAL W: improving the sensitivity of progressive multiple sequence alignment through sequence weighting, position-specific gap penalties and weight matrix choice. *Nucleic Acids Res.* **1994**, *22* (22), 4673−4680.
(90) Yoon, S.-H.; Ha, S.-M.; Kwon, S.; Lim, J.; Kim, Y.; Seo, H.; Chun, J. Introducing EzBioCloud: a taxonomically united database of 16S rRNA gene sequences and whole-genome assemblies. *Int. J. Syst. Evol. Microbiol.* **2017**, *67* (5), 1613−1617.
(91) Antonyraj, C. A.; Koilraj, P.; Kannan, S. Synthesis of delaminated LDH: A facile two step approach. *Chem. Commun.* **2010**, *46* (11), 1902−1904.
(92) Abdel-Hady, E. E.; Mahmoud, R.; Hafez, S. H. M.; Mohamed, H. F. M. Hierarchical ternary ZnCoFe layered double hydroxide as efficient adsorbent and catalyst for methanol electrooxidation. *J. Mater. Res. Technol.* **2022**, *17*, 1922−1941.
(93) Wu, M.; Guo, E.; Li, Q.; Mi, J.; Fan, H. Mesoporous Zn-Fe-based binary metal oxide sorbent with sheet-shaped morphology: Synthesis and application for highly efficient desulfurization of hot coal gas. *Chem. Eng. J.* **2020**, *389*, 123750.

https://doi.org/10.1021/acsomega.4c02133
ACS Omega 2024, 9, 34507−34529

(94) Agarwal, H.; Nakara, A.; Menon, S.; Shanmugam, V. Eco-friendly synthesis of zinc oxide nanoparticles using Cinnamomum Tamala leaf extract and its promising effect towards the antibacterial activity. *J. Drug Delivery Sci. Technol.* **2019**, *53*, 101212.
(95) Philip, D. Synthesis and spectroscopic characterization of gold nanoparticles. *Spectrochim. Acta, Part A* **2008**, *71* (1), 80−85.
(96) Zhao, H.; Maruthupandy, M.; Al-mekhlafi, F. A.; Chackaravarthi, G.; Ramachandran, G.; Chelliah, C. K. Biological synthesis of copper oxide nanoparticles using marine endophytic actinomycetes and evaluation of biofilm producing bacteria and A549 lung cancer cells. *J. King Saud Univ., Sci.* **2022**, *34* (3), 101866.
(97) Jillani, S.; Jelani, M.; Hassan, N. U.; Ahmad, S.; Hafeez, M. Synthesis, characterization and biological studies of copper oxide nanostructures. *Mater. Res. Express* **2018**, *5* (4), 045006.
(98) Felix, S.; Chakkravarthy, R. B. P.; Grace, A. N. Microwave assisted synthesis of copper oxide and its application in electrochemical sensing. In *IOP Conference Series: Materials Science and Engineering*; IOP Publishing, 2015; p 012115.
(99) Rasool, U.; Hemalatha, S. Marine endophytic actinomycetes assisted synthesis of copper nanoparticles (CuNPs): Characterization and antibacterial efficacy against human pathogens. *Mater. Lett.* **2017**, *194*, 176−180.
(100) Nabila, M. I.; Kannabiran, K. Biosynthesis, characterization and antibacterial activity of copper oxide nanoparticles (CuO NPs) from actinomycetes. *Biocatal. Agric. Biotechnol.* **2018**, *15*, 56−62.
(101) Singh, P.; Kim, Y.-J.; Zhang, D.; Yang, D.-C. Biological synthesis of nanoparticles from plants and microorganisms. *Trends Biotechnol.* **2016**, *34* (7), 588−599.
(102) Li, X.; Xu, H.; Chen, Z.-S.; Chen, G. Biosynthesis of nanoparticles by microorganisms and their applications. *J. Nanomater.* **2011**, *2011*, 1−16.
(103) Mahgoub, S. M.; Shehata, M. R.; Abo El-Ela, F. L.; Farghali, A.; Zaher, A.; Mahmoud, R. K. Sustainable waste management and recycling of Zn-Al layered double hydroxide after adsorption of levofloxacin as a safe anti-inflammatory nanomaterial. *RSC Adv.* **2020**, *10* (46), 27633−27651.
(104) Abd Elhaleem, M. B.; Farghali, A. A.; El-Shahawy, A. A.; Abo El-Ela, F. I.; Eldine, Z. E.; Mahmoud, R. K. Chemisorption and sustained release of cefotaxime between a layered double hydroxide and polyvinyl alcohol nanofibers for enhanced efficacy against second degree burn wound infection. *RSC Adv.* **2020**, *10* (22), 13196−13214.
(105) Abboud, Y.; Saffaj, T.; Chagraoui, A.; El Bouari, A.; Brouzi, K.; Tanane, O.; Ihssane, B. Biosynthesis, characterization and antimicrobial activity of copper oxide nanoparticles (CONPs) produced using brown alga extract (Bifurcaria bifurcata). *Appl. Nanosci.* **2014**, *4*, 571−576.
(106) Holzwarth, U.; Gibson, N. The Scherrer equation versus the'Debye-Scherrer equation'. *Green Process. Synth.* **2011**, *6* (9), 534.
(107) Zeng, X.; Yang, Z.; Liu, F.; Long, J.; Feng, Z.; Fan, M. An in situ recovery method to prepare carbon-coated Zn-Al-hydrotalcite as the anode material for nickel-zinc secondary batteries. *RSC Adv.* **2017**, *7* (70), 44514−44522.
(108) Zaher, A.; Taha, M.; Mahmoud, R. K. Possible adsorption mechanisms of the removal of tetracycline from water by La-doped Zn-Fe-layered double hydroxide. *J. Mol. Liq.* **2021**, *322*, 114546.
(109) Salem, S. S.; El-Belely, E. F.; Niedbała, G.; Alnoman, M. M.; Hassan, S. E.-D.; Eid, A. M.; Shaheen, T. I.; Elkelish, A.; Fouda, A. Bactericidal and in-vitro cytotoxic efficacy of silver nanoparticles (Ag-NPs) fabricated by endophytic actinomycetes and their use as coating for the textile fabrics. *Nanomaterials* **2020**, *10* (10), 2082.
(110) Nassar, A.-R. A.; Atta, H. M.; Abdel-Rahman, M. A.; El Naghy, W. S.; Fouda, A. Myco-synthesized copper oxide nanoparticles using harnessing metabolites of endophytic fungal strain Aspergillus terreus: an insight into antibacterial, anti-Candida, biocompatibility, anticancer, and antioxidant activities. *BMC Complementary Med. Ther.* **2023**, *23* (1), 261.
(111) Ponmurugan, P.; Manjukarunambika, K.; Elango, V.; Gnanamangai, B. M. Antifungal activity of biosynthesised copper nanoparticles evaluated against red root-rot disease in tea plants. *J. Exp. Nanosci.* **2016**, *11* (13), 1019−1031.
(112) Bin Mobarak, M.; Hossain, M. S.; Chowdhury, F.; Ahmed, S. Synthesis and characterization of CuO nanoparticles utilizing waste fish scale and exploitation of XRD peak profile analysis for approximating the structural parameters. *Arabian J. Chem.* **2022**, *15* (10), 104117.
(113) Abdel Moaty, S.; Mahmoud, R. K.; Mohamed, N. A.; Gaber, Y.; Farghali, A. A.; Abdel Wahed, M. S.; Younes, H. A. Synthesis and characterisation of LDH-type anionic nanomaterials for the effective removal of doxycycline from aqueous media. *Water Environ. J.* **2020**, *34*, 290−308.
(114) GadelHak, Y.; Salama, E.; Abd-El Tawab, S.; Mouhmed, E. A.; Alkhalifah, D. H. M.; Hozzein, W. N.; Mohaseb, M.; Mahmoud, R. K.; Amin, R. M. Waste Valorization of a Recycled ZnCoFe Mixed Metal Oxide/Ceftriaxone Waste Layered Nanoadsorbent for Further Dye Removal. *ACS Omega* **2022**, *7* (48), 44103−44115.
(115) Qin, Q.; Wu, X.; Chen, L.; Jiang, Z.; Xu, Y. Simultaneous removal of tetracycline and Cu (II) by adsorption and coadsorption using oxidized activated carbon. *RSC Adv.* **2018**, *8* (4), 1744−1752.
(116) Moaty, S. A.; Farghali, A.; Moussa, M.; Khaled, R. Remediation of waste water by Co-Fe layered double hydroxide and its catalytic activity. *J. Taiwan Inst. Chem. Eng.* **2017**, *71*, 441−453.
(117) Du, W.-L.; Niu, S.-S.; Xu, Y.-L.; Xu, Z.-R.; Fan, C.-L. Antibacterial activity of chitosan tripolyphosphate nanoparticles loaded with various metal ions. *Carbohydr. Polym.* **2009**, *75* (3), 385−389.
(118) Ngan, L. T. K.; Wang, S.-L.; Hiep, Đ. M.; Luong, P. M.; Vui, N. T.; Đinh, T. M.; Dzung, N. A. Preparation of chitosan nanoparticles by spray drying, and their antibacterial activity. *Res. Chem. Intermed.* **2014**, *40*, 2165−2175.
(119) Chandrasekaran, M.; Kim, K. D.; Chun, S. C. Antibacterial activity of chitosan nanoparticles: A review. *Processes* **2020**, *8* (9), 1173.
(120) Bukhari, S. I.; Hamed, M. M.; Al-Agamy, M. H.; Gazwi, H. S.; Radwan, H. H.; Youssif, A. M. Biosynthesis of copper oxide nanoparticles using Streptomyces MHM38 and its biological applications. *J. Nanomater.* **2021**, *2021*, 1−16.
(121) Sankar, R.; Manikandan, P.; Malarvizhi, V.; Fathima, T.; Shivashangari, K. S.; Ravikumar, V. Green synthesis of colloidal copper oxide nanoparticles using Carica papaya and its application in photocatalytic dye degradation. *Spectrochim. Acta, Part A* **2014**, *121*, 746−750.
(122) Mortimer, M.; Wang, Y.; Holden, P. A. Molecular mechanisms of nanomaterial-bacterial interactions revealed by omics—the role of nanomaterial effect level. *Front. bioeng. biotechnol.* **2021**, *9*, 683520.
(123) Ahmad, H.; Venugopal, K.; Bhat, A.; Kavitha, K.; Ramanan, A.; Rajagopal, K.; Srinivasan, R.; Manikandan, E. Enhanced biosynthesis synthesis of copper oxide nanoparticles (CuO-NPs) for their antifungal activity toxicity against major phyto-pathogens of apple orchards. *Pharm. Res.* **2020**, *37*, 246.
(124) Ijaz, F.; Shahid, S.; Khan, S. A.; Ahmad, W.; Zaman, S. Green synthesis of copper oxide nanoparticles using Abutilon indicum leaf extract: Antimicrobial, antioxidant and photocatalytic dye degradation activitie. *Trop. J. Pharm. Res.* **2017**, *16* (4), 743−753.
(125) Ma, X.; Zhou, S.; Xu, X.; Du, Q. Copper-containing nanoparticles: Mechanism of antimicrobial effect and application in dentistry-a narrative review. *Front. surg.* **2022**, *9*, 905892.
(126) Santo, C. E.; Taudte, N.; Nies, D. H.; Grass, G. Contribution of copper ion resistance to survival of Escherichia coli on metallic copper surfaces. *Appl. Environ. Microbiol.* **2008**, *74* (4), 977−986.
(127) Gohi, B. F. C. A.; Zeng, H.-Y.; Xu, S.; Zou, K.-M.; Liu, B.; Huang, X. L.; Cao, X.-J. Optimization of znal/chitosan supra-nano hybrid preparation as efficient antibacterial material. *Int. J. Mol. Sci.* **2019**, *20* (22), 5705.
(128) Cheng, H.-M.; Gao, X.-W.; Zhang, K.; Wang, X.-R.; Zhou, W.; Li, S.-J.; Cao, X.-L.; Yan, D.-P. A novel antimicrobial composite: ZnAl-hydrotalcite with p-hydroxybenzoic acid intercalation and its possible application as a food packaging material. *New J. Chem.* **2019**, *43* (48), 19408−19414.
(129) Moaty, S. A.; Farghali, A.; Khaled, R. Preparation, characterization and antimicrobial applications of Zn-Fe LDH against MRSA. *Mater. Sci. Eng., C* **2016**, *68*, 184−193.

https://doi.org/10.1021/acsomega.4c02133
ACS Omega 2024, 9, 34507−34529

(130) Colinas, I. R.; Rojas-Andrade, M. D.; Chakraborty, I.; Oliver, S. R. Two structurally diverse Zn-based coordination polymers with excellent antibacterial activity. *CrystEngComm* **2018**, *20* (24), 3353−3362.
(131) Li, M.; Zhu, L.; Lin, D. Toxicity of ZnO nanoparticles to Escherichia coli: mechanism and the influence of medium components. *Environ. Sci. Technol.* **2011**, *45* (5), 1977−1983.
(132) Radke, L. L.; Hahn, B. L.; Wagner, D. K.; Sohnle, P. G. Effect of abscess fluid supernatants on the kinetics of Candida albicans growth. *Clin. Immunol. Immunopathol.* **1994**, *73* (3), 344−349.
(133) Selvanathan, V.; Aminuzzaman, M.; Tan, L. X.; Win, Y. F.; Guan Cheah, E. S.; Heng, M. H.; Tey, L.-H.; Arullappan, S.; Algethami, N.; Alharthi, S. S.; Sultana, S.; Shahiduzzaman, M.; Abdullah, H.; Aktharuzzaman, M. Synthesis, characterization, and preliminary in vitro antibacterial evaluation of ZnO nanoparticles derived from soursop (Annona muricata L.) leaf extract as a green reducing agent. *J. Mater. Res. Technol.* **2022**, *20*, 2931−2941.
(134) Delgado, K.; Quijada, R.; Palma, R.; Palza, H. Polypropylene with embedded copper metal or copper oxide nanoparticles as a novel plastic antimicrobial agent. *Lett. Appl. Microbiol.* **2011**, *53* (1), 50−54.
(135) Syame, S. M.; Mohamed, W.; K Mahmoud, R.; T Omara, S. Synthesis of Copper-Chitosan Nanocomposites and its Application in Treatment of Local Pathogenic Isolates Bacteria. *Orient. J. Chem.* **2017**, *33* (6), 2959−2969.
(136) Barik, S.; Behera, L.; Badamali, S. K. Assessment of thermal and antimicrobial properties of PAN/Zn-Al layered double hydroxide nanocomposites. *Compos. Interfaces* **2017**, *24* (6), 579−591.
(137) Asha, P.; Deepak, K.; Prashanth, M.; Parashuram, L.; Devi, V. A.; Archana, S.; Shanavaz, H.; Shashidhar, S.; Prashanth, K.; Kumar, K. Y.; et al. Ag decorated Zn-Al Layered Double Hydroxide for adsorptive removal of heavy metals and antimicrobial activity: Numerical Investigations, Statistical analysis and Kinetic studies. *Environ. Nanotechnol., Monit. Manage.* **2023**, *20*, 100787.
(138) Raghunath, A.; Perumal, E. Metal oxide nanoparticles as antimicrobial agents: a promise for the future. *Int. J. Antimicrob. Agents* **2017**, *49* (2), 137−152.
(139) Franci, G.; Falanga, A.; Galdiero, S.; Palomba, L.; Rai, M.; Morelli, G.; Galdiero, M. Silver Nanoparticles as Potential Antibacterial Agents. *Molecules* **2015**, *20* (5), 8856−8874.
(140) Jastrzębska, A. M.; Kurtycz, P.; Olszyna, A.; Karwowska, E.; Miaśkiewicz-Pęska, E.; Załęska-Radziwiłł, M.; Doskocz, N.; Basiak, D. The Impact of Zeta Potential and Physicochemical Properties of T i O 2-Based Nanocomposites on Their Biological Activity. *Int. J. Appl. Ceram. Technol.* **2015**, *12* (6), 1157−1173.
(141) Oñate-Garzón, J.; Manrique-Moreno, M.; Trier, S.; Leidy, C.; Torres, R.; Patiño, E. Antimicrobial activity and interactions of cationic peptides derived from Galleria mellonella cecropin D-like peptide with model membranes. *J. Antibiot.* **2017**, *70* (3), 238−245.
(142) Qi, L.; Xu, Z.; Jiang, X.; Hu, C.; Zou, X. Preparation and antibacterial activity of chitosan nanoparticles. *Carbohydr. Res.* **2004**, *339* (16), 2693−2700.
(143) Panáček, A.; Smékalová, M.; Kilianová, M.; Prucek, R.; Bogdanová, K.; Večeřová, R.; Kolář, M.; Havrdová, M.; Płaza, G. A.; Chojniak, J.; et al. Strong and nonspecific synergistic antibacterial efficiency of antibiotics combined with silver nanoparticles at very low concentrations showing no cytotoxic effect. *Molecules* **2015**, *21* (1), 26.
(144) Moschini, E.; Colombo, G.; Chirico, G.; Capitani, G.; Dalle-Donne, I.; Mantecca, P. Biological mechanism of cell oxidative stress and death during short-term exposure to nano CuO. *Sci. Rep.* **2023**, *13* (1), 2326.
(145) Gupta, G.; Cappellini, F.; Farcal, L.; Gornati, R.; Bernardini, G.; Fadeel, B. Copper oxide nanoparticles trigger macrophage cell death with misfolding of Cu/Zn superoxide dismutase 1 (SOD1). *Part. Fibre Toxicol.* **2022**, *19* (1), 33.
(146) Bukhari, S. I.; Hamed, M. M.; Al-Agamy, M. H.; Gazwi, H. S. S.; Radwan, H. H.; Youssif, A. M. Biosynthesis of Copper Oxide Nanoparticles Using Streptomyces MHM38 and Its Biological Applications. *J. Nanomater.* **2021**, *2021*, 6693302.
(147) Hassan, S. E.-D.; Fouda, A.; Radwan, A. A.; Salem, S. S.; Barghoth, M. G.; Awad, M. A.; Abdo, A. M.; El-Gamal, M. S. Endophytic actinomycetes Streptomyces spp mediated biosynthesis of copper oxide nanoparticles as a promising tool for biotechnological applications. *JBIC, J. Biol. Inorg. Chem.* **2019**, *24*, 377−393.
(148) Rajeshkumar, S.; Nandhini, N. T.; Manjunath, K.; Sivaperumal, P.; Krishna Prasad, G.; Alotaibi, S. S.; Roopan, S. M. Environment friendly synthesis copper oxide nanoparticles and its antioxidant, antibacterial activities using Seaweed (Sargassum longifolium) extract. *J. Mol. Struct.* **2021**, *1242*, 130724.
(149) Balaji, T.; Manushankar, C. M.; Al-Ghanim, K. A.; Kamaraj, C.; Thirumurugan, D.; Thanigaivel, S.; Nicoletti, M.; Sachivkina, N.; Govindarajan, M. Padina boergesenii-Mediated Copper Oxide Nanoparticles Synthesis, with Their Antibacterial and Anticancer Potential. *Biomedicines* **2023**, *11* (8), 2285.
(150) Talebian, S.; Shahnavaz, B.; Nejabat, M.; Abolhassani, Y.; Rassouli, F. B. Bacterial-mediated synthesis and characterization of copper oxide nanoparticles with antibacterial, antioxidant, and anticancer potentials. *Front. bioeng. biotechnol.* **2023**, *11*, 1140010.
(151) Singh, D.; Jain, D.; Rajpurohit, D.; Jat, G.; Kushwaha, H. S.; Singh, A.; Mohanty, S. R.; Al-Sadoon, M. K.; Zaman, W.; Upadhyay, S. K. Bacteria assisted green synthesis of copper oxide nanoparticles and their potential applications as antimicrobial agents and plant growth stimulants. *Front. Chem.* **2023**, *11*, 1154128.
(152) Fouda, A.; Hassan, S. E.-D.; Eid, A. M.; Awad, M. A.; Althumayri, K.; Badr, N. F.; Hamza, M. F. Endophytic bacterial strain, Brevibacillus brevis-mediated green synthesis of copper oxide nanoparticles, characterization, antifungal, in vitro cytotoxicity, and larvicidal activity. *Green Process. Synth.* **2022**, *11* (1), 931−950.
(153) Kouhkan, M.; Ahangar, P.; Babaganjeh, L. A.; Allahyari-Devin, M. Biosynthesis of copper oxide nanoparticles using Lactobacillus casei subsp. casei and its anticancer and antibacterial activities. *Curr. Nanosci.* **2020**, *16* (1), 101−111.
(154) Asha, P. K.; Deepak, K.; Prashanth, M. K.; Parashuram, L.; Devi, V. A.; Archana, S.; Shanavaz, H.; Shashidhar, S.; Prashanth, K. N.; Kumar, K. Y.; Raghu, M. S. Ag decorated Zn-Al layered double hydroxide for adsorptive removal of heavy metals and antimicrobial activity: Numerical investigations, statistical analysis and kinetic studies. *Environ. Nanotechnol., Monit. Manage.* **2023**, *20*, 100787.

https://doi.org/10.1021/acsomega.4c02133
ACS Omega 2024, 9, 34507−34529